Low-T eclogite in the Dabie Terrane of China: Petrological and isotopic constraints on fluid activity and radiometric dating

ARTICLE *in* CONTRIBUTIONS TO MINERALOGY AND PETROLOGY · NOVEMBER 2004

Impact Factor: 3.48 · DOI: 10.1007/s00410-004-0616-9

Contrib Mineral Petrol (2004) 148: 443–470
DOI 10.1007/s00410-004-0616-9

ORIGINAL PAPER

Xu-Ping Li · Yong-Fei Zheng · Yuan-Bao Wu
Fukun Chen · Bing Gong · Yi-Liang Li

Low-T eclogite in the Dabie terrane of China: petrological and isotopic constraints on fluid activity and radiometric dating

Received: 13 March 2004 / Accepted: 18 August 2004 / Published online: 2 October 2004

Abstract While extensive studies have demonstrated fluid release during subduction of oceanic crust, little attention has been paid to fluid activity during subduction and exhumation of continental crust. Abundant occurrence of quartz veins within eclogites in the Dabie-Sulu orogenic belt of China provides us with an opportunity to study the origin and role of vein-forming fluids with respect to heat and mass transfer during ultrahigh pressure (UHP) metamorphism and its relevant processes. This study focuses on kyanite-quartz vein that occurs as polycrystalline aggregates within the low-T eclogite in the Dabie terrane, which are interpreted as pseudomorphs after former porphyroblasts of lawsonite. Coesite pseudomorphs were found for the first time in eclogite garnet, resulting in a revised estimate of peak P–T conditions at 670°C and 3.3 GPa for the eclogite and thus upgrading the high-P unit to an UHP unit. On the basis of the relationship between calculated P–T path and metamorphic reactions as well as the absence of foliation texture, and undulose extinction of quartzes in the vein, we conclude that lawsonite breakdown into kyanite–quartz–zoisite assemblage took place at the onset of exhumation subsequent to peak pressure. Retrograde metamorphism caused O and H isotope disequilibria between some of the minerals, but the fluid for retrograde reactions was internally buffered in stable isotope compositions. Zircon U–Pb dating and whole-rock Nd–Sr isotope analyses indicate that eclogite protolith is the paleoceanic basalt that was derived from the depleted mantle by magmatism at about 1.8 to 1.9 Ga but experienced hydrothermal alteration by surface waters. The altered basalt underwent UHP metamorphism in the Triassic that caused fluid release for zircon growth/overgrowth not only at about 242 ± 3 Ma prior to the onset of peak pressure but also at about 222 ± 4 Ma during decompression dehydration by lawsonite breakdown and hydroxyl exsolution in the low-T/UHP eclogite. Consistent ages of 236.1 ± 4.2 Ma and 230 ± 7 Ma were obtained from mineral Sm–Nd and Rb–Sr isochron dating, respectively, indicating attainment and preservation of Nd and Sr isotope equilibria during the Triassic UHP eclogite-facies metamorphism. Ar–Ar dating on paragonite from the eclogite gave consistent plateau and isochron ages of 241.3 ± 3.1 Ma and 245.5 ± 9.8 Ma, respectively, which are interpreted to date paragonite crystallization during the prograde eclogite-facies metamorphism. The timing of peak UHP metamorphism for the low-T eclogite is constrained at sometime prior to 236.1 ± 4.2 Ma. Thus the termination age of peak UHP metamorphism may be different in different slices of deep-subducted slab.

Editorial Responsibility: J.L.R. Touret

X.-P. Li · Y.-F. Zheng (✉) · Y.-B. Wu · B. Gong · Y.-L. Li
School of Earth and Space Sciences,
University of Science and Technology of China,
Hefei, 230026, China
E-mail: yfzheng@ustc.edu.cn

X.-P. Li
School of Earth Sciences and Resources,
China University of Geosciences,
Beijing, 100083, China

Y.-B. Wu
Beijing Ion Microprobe Center,
Chinese Academy of Geological Sciences,
Beijing, 100037, China

F. Chen
Laboratory for Radiogenic Isotope Geochemistry,
Institute of Geology and Geophysics,
Chinese Academy of Sciences,
Beijing, 100029, China

Introduction

Fluid activity in geological processes at subduction zones is very important for understanding a wide spectrum of phenomena including ultrahigh pressure (UHP) metamorphism, syn-collisional magmatism and seismicity. It is also a key to understanding the evolution of the Earth, including the global circulation of water, the fate of deep-subducted slab, the origin of igneous rocks

in collisional orogenic belts, and recycling of oceanic and continental crusts. In particular, metamorphic devolatilization and anatexis of subducted sediments and hydrothermally altered crust are vital to magmatism of syn-subduction versus syn-exhumation with respect to the peak metamorphic event. Although metamorphic fluids are well known to play important roles in geochemical cycling during subduction of young and hot oceanic crust, it is less known whether devolatilization and fluid mobility are also active during subduction and exhumation of old and cold continental crust.

Veins are among the most easily recognized structures in high-grade metamorphic rocks. Veins form as minerals precipitate from solutions and fill up cracks. Quartz veins are the record of metamorphic fluid system that involved fracture flow in the direction of decreasing temperature or pressure. Detailed petrological, fluid inclusion and stable isotope studies indicate that in some occurrences, veins were deposited from fluids that were generated locally, whereas in other places fluids were derived from external sources (e.g., Henry et al. 1996; Matthews et al. 1996; van Haren et al. 1996; Austrheim 1998; Cartwright and Buick 2000; Yardley et al. 2000; Zheng et al. 2003a). The occurrence of veins within eclogites, which are usually considered as ''dry'' rocks, is of particular interest since it may shed light on the nature and amount of fluid present during HP and UHP metamorphism.

Quartz, kyanite and zoisite/clinozoisite aggregates are abundant in kyanite–quartz veins within HP and UHP eclogites in the Dabie-Sulu orogenic belt of China which has been identified as one of the largest UHP metamorphic belts in the world (e.g., Wang et al. 1995; Cong 1996; Liou et al. 1996). This study focuses on kyanite-quartz vein and associated low-T eclogite in the southern part of the Dabie terrane, involving the breakdown of lawsonite into kyanite–zoisite–quartz aggregate at the onset of exhumation. Lawsonite-bearing low-T eclogite has been found in well-known and well developed low-T/high-P metamorphic rocks from eastern Corsican along the southern extension of the Alpine chain (Caron and Pequignot 1986). And more occurrences of pseudomorphs after lawsonite have been reported from the Alps and Southern Urals (Barnicoat and Fry 1986; Barnicoat 1988; Schulte and Sindern 2002). But the mineral assemblage of kyanite–zoisite–quartz as pseudomorph after lawsonite in response to initial exhumation, however, is first reported here.

This paper presents an integrated study of petrology, zircon U–Pb, mineral Sm–Nd and Rb–Sr, and paragonite Ar–Ar dating, whole-rock Nd–Sr and mineral O–H isotopes in kyanite–quartz veins and host eclogites in the Huangzhen-Zhujiachong area of South Dabie. The texture and mineral assemblage from millimeter veins of this study as well as P–T conditions estimated suggest that the veins were formed within the low-T/UHP eclogites in the stage of initial exhumation. Vein-forming fluid was likely derived from the local host-eclogites by the decomposition of hydrous minerals such as lawsonite due to pressure decrease. Thus the fluid was provided by the hydrous mineral via exhumation-driven dehydration and fluid flow during the initial exhumation that occurred along the pressure gradient. The present study demonstrates that devolatilization and fluid flow are also active during continental subduction and exhumation, which may play a key role in geochemical recycling during subduction of continental crust.

Geological setting

The Dabie-Sulu orogenic belt in east-central China was formed by the continental collision between the Yangtze and the Sino-Korean plates in the Triassic (e.g., Wang et al. 1995; Cong 1996; Liou et al. 1996; Li et al. 1999; Zheng et al. 2003a). The regional geology of this belt has been described in many publications and thus is not repeated here in detail. The Dabie terrane is a major segment consisting of a series of fault-bounded metamorphic units in the western part of the orogenic belt. From north to south, they can be divided further as follows: (1) the Beihuaiyang low-grade metamorphic unit, (2) the North Dabie high-T/high-P amphibolite/granulite-facies unit, (3) the Central Dabie medium-T/UHP eclogite-facies unit, (4) the South Dabie low-T/high-P eclogite-facies unit, and (5) the Susong low-T/high-P blueschist/amphibolite-facies unit (Fig. 1). A combined study of stable isotopes and fluid inclusions in HP to UHP eclogites and gneisses from the Dabie-Sulu orogenic belt demonstrates that fluid activity is very small in the peak UHP metamorphic stage and that retrograde metamorphism during exhumation is characterized by internally buffered fluid in chemical and isotopic compositions (Zheng et al. 1998, 1999, 2003a; Fu et al. 1999, 2001, 2002, 2003a b; Xiao et al. 2000, 2002).

On the basis of petrological studies, Okay (1993) divided the eclogite zones in the eastern part of the Dabie terrane into two units: one is the northern MT/UHP (''hot'') eclogite that is characterized by higher metamorphic temperatures, the other is the southern coesite- and diamond-free LT/HP (''cold'') eclogite that was metamorphosed at relatively lower temperatures. The boundary between the two units is located south of the Hualiangting Reservoir (Fig. 1). Following the subdivision of Wang et al. (1992) to separate the eclogite units with distinctly different tectono-metamorphic histories, similarly, Carswell et al. (1997) termed them the South Dabie high-P unit and the Central Dabie ultrahigh-P unit, respectively (Fig. 1). Zhai et al. (1995) pointed out that the country rocks of the ''hot'' eclogite are generally garnet-bearing granitic orthogneiss, paragneiss, marble, and ultramafics, whereas the country rocks of the ''cold'' eclogite are principally magnetite-bearing metasandstone and thus typically a kind of parametamorphic rock. The most important evidence for such a subdivision is that so far no UHP index mineral (e.g., coesite or micro-diamond) has been identified in the ''cold'' eclogite.

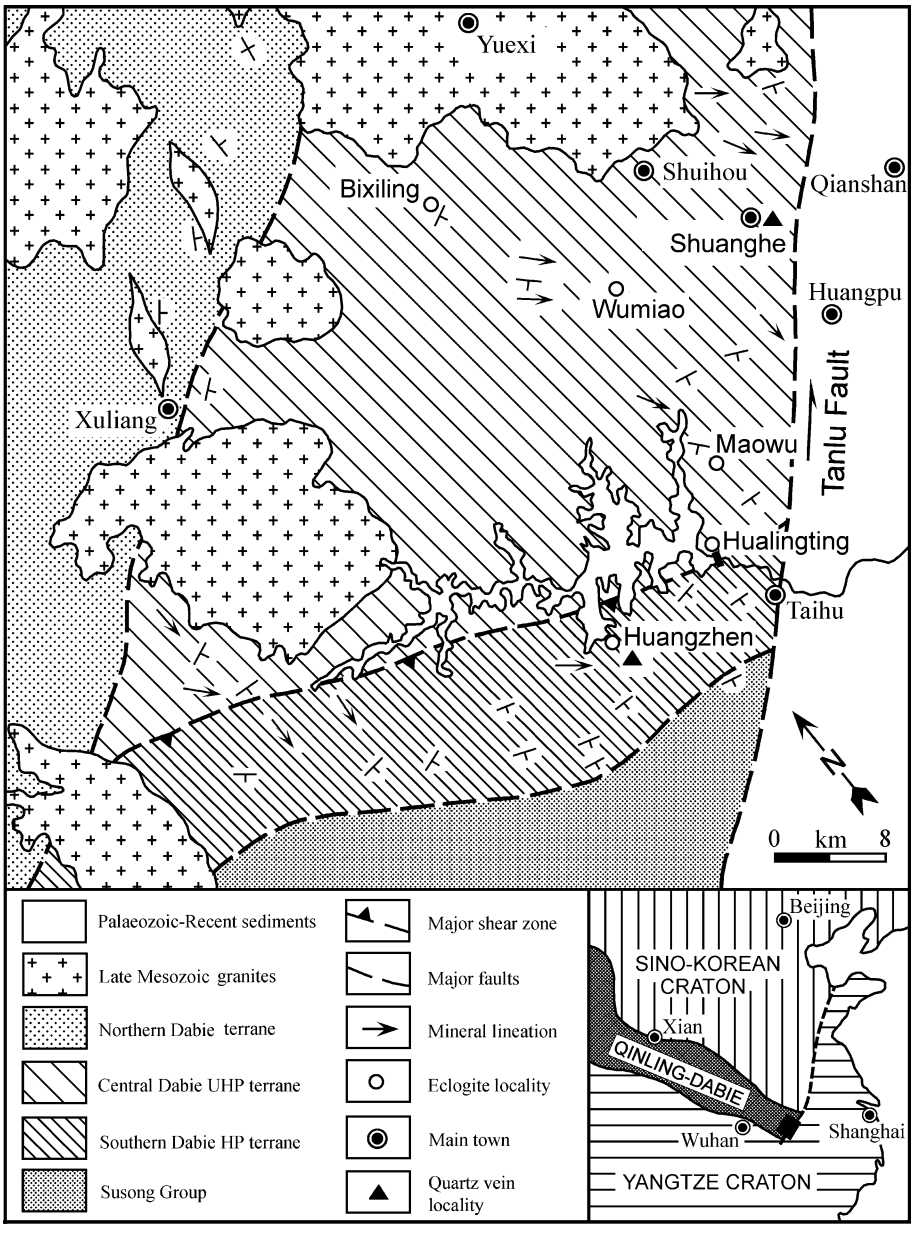

Fig. 1 Sketch map of simplified geology in the southeastern part of the Dabie terrane (revised after Carswell et al. 1997). *Insert* indicates the location of the study-area map at the eastern end of the Qinling-Dabie orogenic belt between the Sino-Korean and Yangtze plates

The present study deals with the low-T eclogite unit between MT/UHP eclogite and LT/HP blueschist units. Samples used in this study were collected from the Huangzhen-Zhujiachong area in the South Dabie low-T/high-P unit (Fig. 2). Previous studies on eclogites in this area suggested the absence of coesite and the presence of sodic amphibole. Metamorphic conditions were determined to be 650–700°C and 1.8 GPa by one group (Zhai et al. 1995; Castelli et al. 1998), or 570–650°C and 1.8–2.5 GPa by the other (Wang et al. 1992; Okay 1993; Carswell et al. 1997; Franz et al. 2001; Xiao et al. 2002). The low-T eclogites were commonly so called because of the low apparent temperatures by cation partitioning geothermometry. A prominent feature of the eclogites is significant retrogression, resulting in considerable disequilibrium O isotope fractionations between the eclogite minerals (Zheng et al. 1999, this study).

Eclogites in the Huangzhen-Zhujiachong area are commonly cut by veins that are usually dominated by quartz, garnet, zoisite and kyanite, and that range in width from submillimeters to several decimeters (Wang et al. 1992; Okay 1993; Carswell et al. 1997; Castelli et al. 1998; Franz et al. 2001; Li et al. 2001). Quartz veins are much more abundant in the LT/HP eclogite of South Dabie than in the MT/UHP eclogites of Central Dabie. Sampled eclogites are layered ones interbedded with eclogite and garnet amphibolite, and hosted by biotite paragneiss. The light quartz–kyanite veins consisting of garnet, kyanite, zoisite, quartz and white mica are parallel to dark eclogites. Reaction zone, mono-mineral zone, or alteration zone are absent between the vein and the hosted eclogite, suggesting a chemical equilibrium between them (Barnicoat 1988). The occurrence of quartz veins across the eclogites in this area witness the

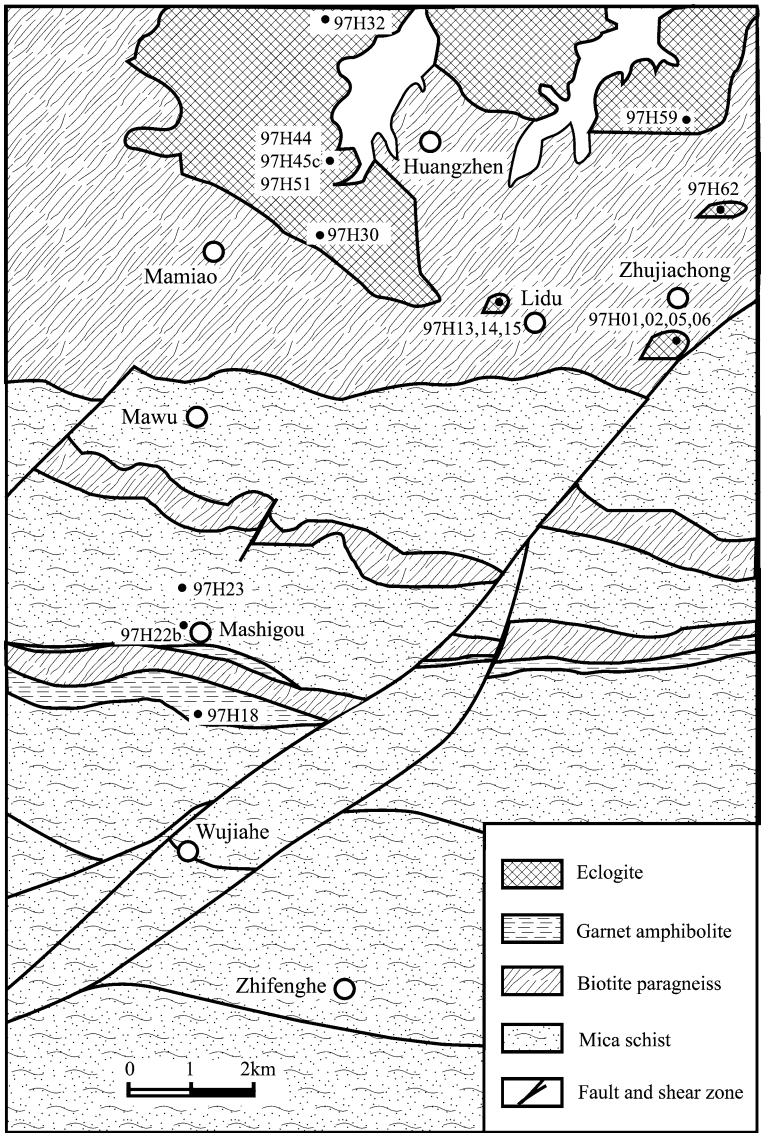

Fig. 2 Sketch map of simplified geology in the Huangzhen-Zhujiachong area with sample locality

channelled flow of metamorphic fluid that may be caused by structural shearing and fracturing during initial exhumation.

Analytical methods

Mineral preparation and chemistry

Individual minerals were separated by conventional magnetism and heavy-liquid techniques, and then handpicked under a binocular microscope to purity generally better than 99%. Mineral chemistry was analyzed by using a JXA-8800R electronic microprobe at Peking University, operated at an acceleration voltage of 15 kV and a beam current of 20 nA. The abbreviation of minerals takes from Kretz (1983).

Zircon U–Pb dating

Zircon U–Pb dating was performed by the SIMS technique that employed the sensitive high-resolution ion microprobe (SHRIMP II) at the Beijing Ion Microprobe Center in the Chinese Academy of Geological Sciences. Instrumental conditions and data acquisition were generally described by Compston et al. (1992) and Williams (1998). The U–Pb isotope data were selected in sets of five scans throughout the masses, and a reference zircon TEM (417 Ma) was analyzed every fourth analysis. The measured U, Th and Pb abundances as well as Pb isotope ratios were corrected against the reference zircon SL13 (572 Ma). Common Pb was corrected using the measured ^{204}Pb, and errors are reported with 1σ error; error in standard calibration was 0.33% (not included in the above errors but required when comparing data from different mounts). The data were treated following

Compston et al. (1992) with the ISOPLOT program of Ludwig (2001), and plotted on the conventional Wetherill-type concordia diagram in $^{206}Pb/^{238}U$ vs. $^{207}Pb/^{235}U$ space.

Mineral Sm–Nd and Rb–Sr dating

Mineral Sm–Nd and Rb–Sr analyses were carried out using isotope dilution techniques at the Univerity of Tuebingen, Germany. Mineral powders were completely decomposed in a mixture of HF–$HClO_4$ for Nd–Sr isotope analysis. Chemical separation and isotopic measurements were conducted following the procedures outlined in Hegner et al. (1995). Sr and LREE were separated in quartz columns with a 5-ml resin bed of AG 50 W-X12, 200–400 mesh. Nd was separated from Sm in quartz columns using 1.7 ml Teflon powder coated with HDEHP as the cation exchange medium. Procedural blanks were <200 pg for Sr and $\sim$30 pg for Nd. Nd and Sr isotope ratios were in static data collection mode with a Finnigan MAT-262 mass spectrometer. Sr was loaded with a Ta–HF activator on a single W filament and Nd was loaded as phosphates and measured in a Re double filament configuration. $^{143}Nd/^{144}Nd$ ratios were normalized to $^{146}Nd/^{144}Nd = 0.7219$ and $^{87}Sr/^{86}Sr$ ratios to $^{86}Sr/^{88}Sr = 0.1194$. During this study, analyses of Nd standard (Ames) yielded $^{143}Nd/^{144}Nd = 0.512129 \pm 11$ ($n = 5$), while Sr standard (NBS 987) yielded $^{87}Sr/^{86}Sr = 0.710236 \pm 7$ ($n = 4$). Sm–Nd and Rb–Sr isochron calculations were made using the regression programs of ISOPLOT (Ludwig 2001). Input errors used in age computations are: $^{147}Sm/^{144}Nd = 0.2\%$, $^{143}Nd/^{144}Nd = 0.005\%$, $^{87}Rb/^{86}Sr = 2\%$ and $^{87}Sr/^{86}Sr = 0.01\%$.

Mineral Ar–Ar dating

Mica Ar–Ar dating was carried out by the step-heating technique at the Institute of Geology in the Chinese Academy of Geological Sciences in Beijing (Chen et al. 2002). The dried samples and the standard samples were wrapped by a pure Al foil and then were irradiated for 60 h under fast neutrons in channel H8 of the Swimming Pool Reactor at the Institute of Atomic Energy, Chinese Academy of Sciences in Beijing. The integrated neutron flux is about 1.3×10^{18} ncm^{-2}. The samples were heated at different temperatures to release gases. Argon isotopic measurements were carried out on a MM-1200B mass spectrometer with a 17-stage Be-Cu electron multiplier. All data of measured ^{40}Ar, ^{39}Ar, ^{37}Ar and ^{36}Ar were corrected for mass discrimination, irradiation induced mass interference, atmospheric Ar component, blanks and so on using the following parameters: $(^{36}Ar/^{37}Ar)_{Ca} = 0.0002389$; $(^{40}Ar/^{39}Ar)_{k} = 0.004782$; $(^{39}Ar/^{37}Ar)_{Ca} = 0.000806$. All ^{37}Ar were corrected for radiogenic decay (half-life 35.1 days). Plateau and isochron ages were calculated using the ISOPLOT program of Ludwig (2001) with uncertainties at 2σ deviations. The monitor used was a national standard biotite ZBH-25, whose age is 132.7 Ma and K content is 7.6%.

Whole-rock Nd and Sr isotopes

The determination of whole-rock Sm–Nd and Rb–Sr isotope ratios as well as Sm, Nd, Rb and Sr concentrations were conducted by the conventional isotope dilution techniques at the Open Laboratory of Isotope Geology in the Chinese Academy of Geological Sciences, Beijing. The Nd and Sr isotope ratios were measured on a Finnigan MAT-261 mass spectrometer. Corrections of isotopic mass fractionation of Nd and Sr were made with $^{146}Nd/^{144}Nd = 0.7219$ and $^{86}Sr/^{88}Sr = 0.1194$, respectively. The $^{143}Nd/^{144}Nd$ ratios determined with the Nd isotope standard J.M. Nd_2O_3 and La Jolla are 0.511125 ± 10 and 0.511849 ± 9 (2σ), respectively; the $^{143}Nd/^{144}Nd$ ratio determined with the continental basalt standard BCR-1 is 0.512643 ± 12 (2σ), and the $^{87}Sr/^{86}Sr$ ratio determined with the Sr isotope standard NBS-987 is 0.710250 ± 10 (2σ).

Mineral O and H isotopes

O isotope analysis was carried out by the laser fluorination technique using a 25 W MIR-10 CO_2 laser at Hefei (Sharp 1990; Zheng et al. 2002), differing from the previous analysis by the conventional BrF_5 method (Clayton and Mayeda 1963; Zheng et al. 1999; Li et al. 2001). In the present study, O_2 was directly transferred to a Delta + mass spectrometer for the measurement of $^{18}O/^{16}O$ and $^{17}O/^{16}O$ ratios. O isotope data are reported as parts per thousand differences (‰) from the reference standard VSMOW in the $\delta^{18}O$ notation. Two reference minerals were used: $\delta^{18}O = 5.8‰$ for UWG-2 garnet (Valley et al. 1995) and $\delta^{18}O = 5.2‰$ for SCO-1 olivine (Eiler et al. 1995). Errors for repeat measurements of each standard on a given day were better than $\pm 0.1‰$ (1σ) for $\delta^{18}O$.

H isotope analysis was accomplished by liberating OH from hydroxyl-bearing silicates at the high temperature and then converted to H_2 by reaction with hot zinc metal at 400° (Friedman 1953). D/H ratios were measured in a MAT-251 mass spectrometer at Beijing and reported in the δD notation relative to the VSMOW standard. Repeated analyses yield the reproducibility of better than $\pm 3‰$ for δD. A reference sample of water was used with a δD value of $-62‰$ for the National Standard of China QYTB and a reference sample of biotite was used with a δD value of $-66‰$ for the International Standard NBS-30.

Petrography

The samples used in this study are located south of the Hualiangting Reservoir (Figs. 1 and 2) and were taken from the Huangzhen-Zhujiachong area in South Dabie (Figs. 1 and 2). Relationships in field occurrence between

investigated vein and host eclogite for outcrops at Huangzhen is largely dominated by eclogite and intercalated kyanite–quartz veins. Sometimes the rocks show intergrowth of eclogite and veins in microscope scale. The outcrops close to Zhujiachong, 2∼3 km to the southern boundary with the coesite-eclogite zone, show several intergrowth kyanite–quartz veins within fresh eclogites. The size of the quartz veins strongly varies from <1 to >5 cm. The distribution and orientation of mineral phases in these veins are highly variable. Four representative sections within this network of veins were investigated. Besides quartz, the veins are made up of kyanite, paragonite, zoisite, rutile as well as garnet and omphacite. The represented samples used for this study are listed in Table 1, and described as following three represented groups.

Intergrowth samples of eclogite and quartz–kyanite veins in microscope scale

The representative samples are 97H51 and 97H59, containing both hosted eclogite and quartz–kyanite veins that are the most important rocks in this study. The contact between eclogite and vein are clear. The veins, intercalated with hosted eclogite, are of 2 to >10 mm width in the thin sections. The eclogite consists of anhedral omphacite, euhedral porphyroblasts of garnet, zoisite/clinozoisite, paragonite and retrogressive amphibole. Accessory minerals are rutile, apatite and retrograde titanite. Coesite or its quartz pseudomorph were observed within garnets, and recognized by the occurrence of radial fractures in hosted garnet around the pseudomorph (Fig. 3). Relict coesite could be distinguished from quartz by its higher birefringence, and multi-grain quartz under crossed nicols.

Most garnets are rimmed by retrogressive corona of sodic amphibole. Kyanite was observed in contact with garnet and omphacite or within the omphacite as inclusion, and associated with coesite-bearing garnet. Paragonite occurs in both eclogite sections and veins. In the hosted eclogite, kyanite sometimes consists of core and is rimed by omphacite, which suggests a reaction of paragonite = kyanite + omphacite + H_2O.

The quartz–kyanite veins are made of over half volume of quartz, garnets (10–15 vol%), zoisite/clino-

Table 1 Investigated samples of metamorphic rocks at Huangzhen in South Dabie

Sample no.	Lithology	Mineral assemblages (vol%)	
		Host rock	Vein
97H01	Quartz vein		Qtz (80%), Ms (10%); minor minerals: Omp, Grt, Ky, Czo, Tlc and Rt
97H02	Eclogite	Omp 30%, Grt 40%, Amph 10%; minor minerals: Ms, Zo, Qtz, Ky, Rt	Qtz (70%), Pa (10%), Grt (10%); minor minerals: Omp, Ky, Czo and Rt
97H05	Eclogite	Omp 30%, Grt 35%, Amph 15%; minor minerals: Ms, Zo, Qtz, Ky, Rt	Qtz (90 vol%), Ms (<10 vol%); minor minerals: Omp, Grt, ky, Tlc, Rt
97H06	Eclogite	Omp 30%, Grt 40%, Amph 10%; minor minerals: Pa, Zo, Qtz, Ky, Rt	
97H13 97H14	Eclogite	Omp 35%, Grt 15% and Czo (25%), Pa 10%; minor minerals: Qtz, Pl, Rt	Qtz (90 vol%), Pa (<10 vol%); minor minerals: Omp, Grt, Rt
97H15	Eclogite	Omp 30%, Grt 25%, Amph 10%, Czo 20%; minor minerals: Pa, Qtz, Rt, others	Qtz (80 vol%), Pa (10 vol%); minor minerals: Omp, Grt, Ky, Czo, Rt
97H30	Eclogite	Omp 40%, Grt 40%, Pa 5% Qtz 10%; minor minerals: Ky, Czo	
97H32	Eclogite	Omp (45%), Grt(40%), Qtz (5%); minor minerals: Pa, Rt	
97H45c	Eclogite	Omp (25%), Amph (20%), Grt(30%), Zo (10%), Qtz (%), Ms (%), Rt	
97H51ev|rm [a]	Eclogite	Omp 45%, Grt 40%; minor minerals: Amph, Pa, Zo, Qtz, Ky, Rt	Qtz 65%, Grt 15%; Czo 10%, Ky 8%; minor minerals: Pa, Omp, Rt
97H59ev	Eclogite	Omp 45%, Grt 40%; minor minerals: Amph, Pa, Zo, Qtz, Ky, Rt	Qtz 60%, Grt 15%; Czo 15%, Ky 5%; minor minerals: Pa, Omp, Rt
97H62	Eclogite	Omp 45%, Grt 40%, Qtz 10%; minor minerals: amph, Rt	
97H18	Amphibolite	Amph (40%), Grt(35%), Bi(10%); minor minerals: Qtz, Pl, Ms, Ttn	
97H22b	Amphibolite	Amph (35%), Grt(35%), Bi(15%); minor minerals: Qtz, Pl, Ms, Czo	
97H23	Gneiss	Qtz 60%, Ms 15%, Pl 15%, Mgt 10%	
97H44	Gneiss	Qtz (%),Ms (%), Bi (%), Grt(%), Ep (%)	

[a] "ev" refer to the eclogite host and vein intercalated appear on one sample

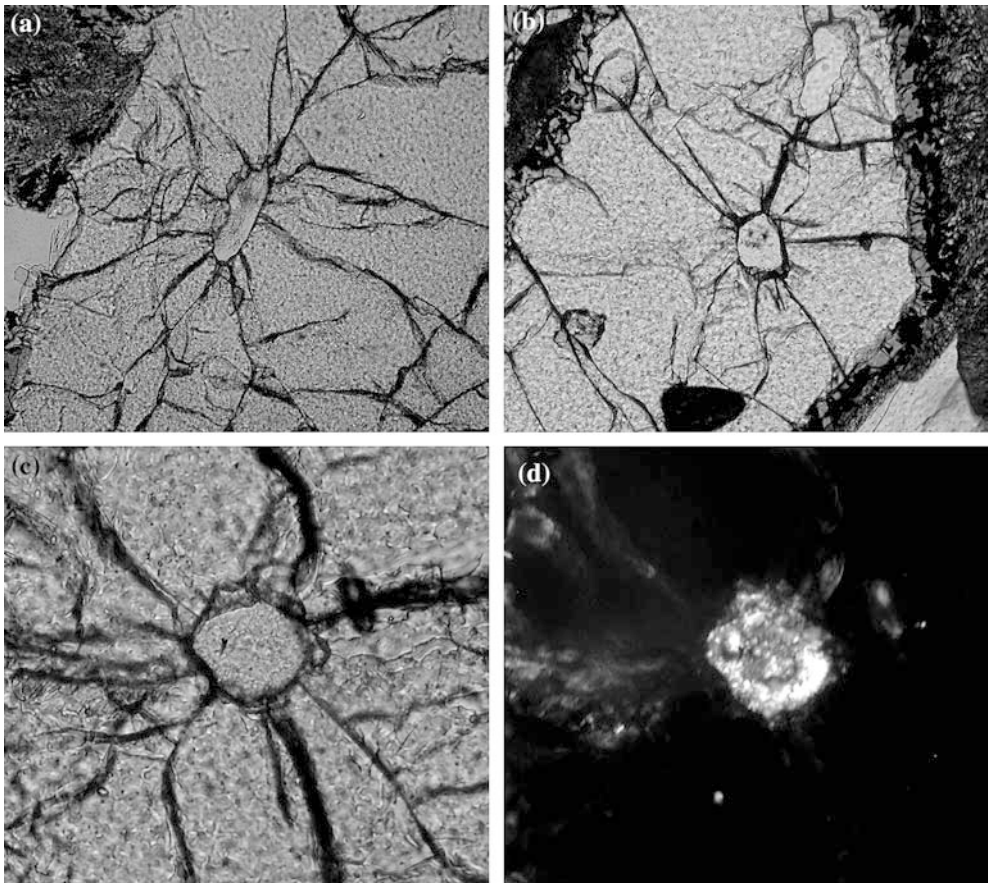

Fig. 3 Coesite pseudomorph/quartz radiated texture under different polarized lights from low-T eclogites in South Dabie. (**a**) and (**b**) are two occurrences under plainlight conditions; (**c**) and (**d**) are the same occurrence under single and crossed polarlights, respectively

zoisite (5–10 vol%), omphacite (< 5 vol%), and kyanite (5–10 vol%), and minor other minerals. They are locally characterized by the occurrence of abundant millimeter-sized mineral aggregations, which appear to be pseudomorphs after earlier porphyroblastic mineral with a prismatic habit (Fig. 4). The pseudomorphs usually consist of single to two grains of kyanite, fine-multigrain zoisite/clinozoisite and very fine-grained quartz, which is mostly included in the kyanite with a random orientation (Fig. 4a–c). In the thin sections, such three minerals as kyanite, zoisite/clinozoisite and quartz occur in close proximity and are assumed to be in texture equilibrium. Based on the texture and the mineral assemblages, the Ky–Zo–Qtz aggregates are considered to be breakdown product after lawsonite, which usually shows a typical prismatic habit (Fig. 4). Lawsonite pseudomorphs or Ky–Zo–Qtz aggregates frequently occur in the veins and take account to about 7 vol%. Garnet in the veins shows grain sizes of 0.5–1 mm, which are smaller than those (1–3 mm) in the host eclogite. Foliation and sutured boundaries of quartz are not well developed in both host eclogite and quartz veins. No undulose extinction, kink-bands and fractures are clearly observed in both eclogite and quartz veins.

Individual eclogite and kyanite–quartz vein

These are the samples consisting of separated eclogites and veins. Most of the investigated samples belong to this category. The veins are variable from 2 mm to 1 m on the outcrops so that they consist of single vein samples in comparison to the first group samples.

The eclogite minerals show a remarkable variability of pervasively retrograded texture. Omphacite is usually replaced by very fine-grained symplectites that consist of retrogressive sodic amphibole and feldspar. Some samples show a stronger retrograde texture than the others so that amphibole and sometimes subsequently biotite were crystallized from symplectites. The omphacite continued to breakdown to cause an increase in amphibole minerals. Other minerals include zoisite, plagioclase, rutile and retrograde titanite and sometimes magnetite. No coesite pseudomorph has been observed in this group of samples. Paragonite occurs in the following three forms: (1) as a relic in the core of kyanite with size of about 0.2 mm, and kyanite in turn is rimed by omphacite, (2) overprinted by early clinozoisite and showing large grains (> 3 mm), (3) as a relic in the amphibole, which was retrograded from omphacite. Thus the paragonite was mainly formed by prograde HP

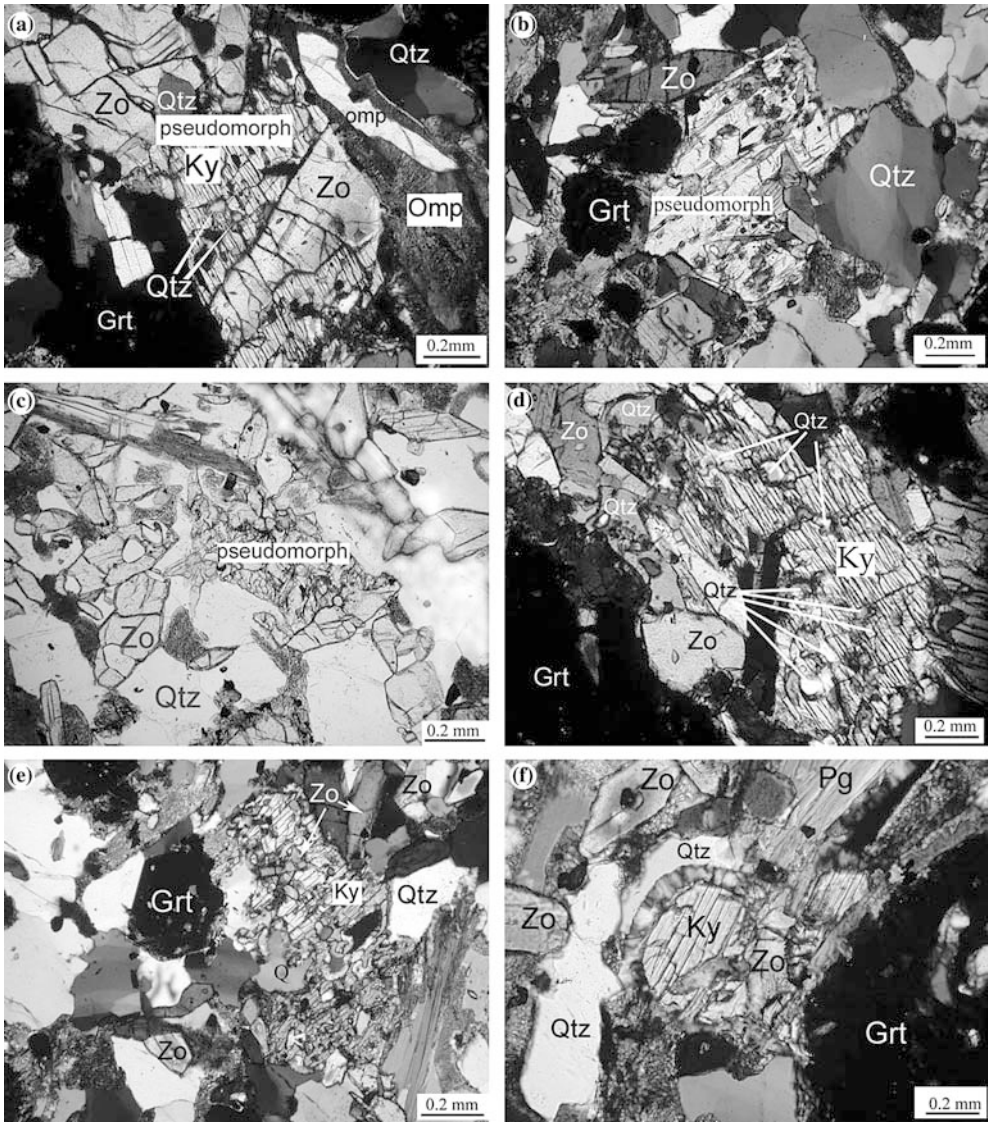

Fig. 4 Micrographs of textures from quartz–kyanite vein and associated eclogite from the Huangzhen-Zhujiachong in South Dabie. Mineral aggregates of Ky + Zo + Qtz as pseudomorph after lawsonite with a prismatic habit. **a** Pseudomorph under cross-polarized light consisting of two grains of zoisite, two grains of kyanite and many fine grains of quartz, **b** pseudomorph under cross-polarized light consisting of single grain kyanite and multi, fine-grain zoisite and quartz, **c** pseudomorph under plane-polarized light consisting of multi, fine-grain kyanite, zoisite and quartz, **d** pseudomorph under cross-polarized light consisting of multi, fine-grain zoisite, single grain kyanite and many fine grain quartzs included in kyanite, **e** aggregate of presumed pseudomorph under cross-polarized light, **f** symplectitic rim of kyanite and aggregate of presumed pseudomorph under cross-polarized light

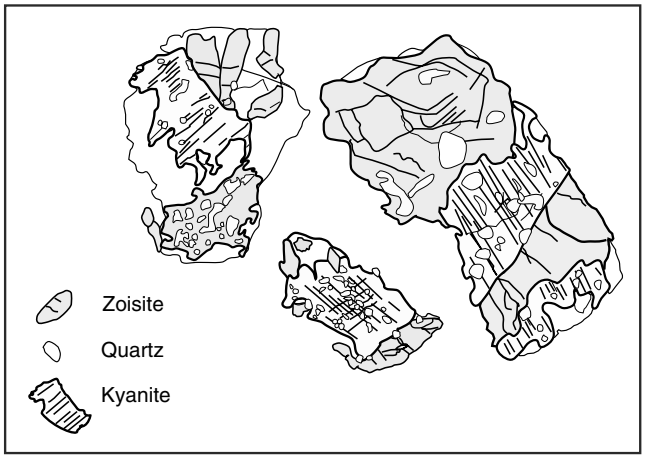

Fig. 5 Thin section sketch of pseudomorphs of mineral aggregates of Ky + Zo + Qtz after lawsonite in eclogites from the Huangzhen-Zhujiachong area in South Dabie

metamorphism during subduction. No paragonite with obvious retrogressive texture was found in the eclogites.

A few samples contain significant amounts of clinozoisite up to about 25 vol%, much lower amounts of garnet and the same amounts of omphacite as the other samples (97H13, 97H14 and 97H15). No kyanite has been found in the samples. Both eclogite and vein display a mylonitic texture with elongated oriented minerals along the direction of vein. Elongated crystals of clinozoisite could reach up to 3∼5 mm in size. At the boundary between eclogite and vein, deformed polycrystallized quartz with foliation shows a subgrain rotation recrystallization. Quartz in the vein exhibits sutured contact with each other at the boundaries.

Veins are heterogeneous in texture and mineral assemblage, consisting of granoblastic quartz grains, randomly oriented needle-like white paragonite flakes (97H01 and 97H02), anhedral omphacite, zoisite, kyanite, garnet and rutile with a porphyroblastic tex-

Table 2 Chemical composition of representative garnets in quartz veins and eclogites at Huangzhen in South Dabie

	97H59-51	97H59-52	97H59-53	97H59-54	97H59-55	97H59-56	97H59-57	97H59-58	97H05-21	97H05-22	97H05-23	97H15-11	97H15-16	97H59-11	97H59-12	97H02-11	97H02-12
	Garnet in eclogite													Garnet in vein			
SiO_2	39.53	39.54	38.68	38.86	38.79	39.34	39.23	38.97	39.43	39.41	39.15	39.03	37.46	39.49	39.22	38.94	40.03
TiO_2	0.00	0.04	0.02	0.03	0.07	0.00	0.04	0.00	0.05	0.47	0.07	0.00	0.00	0.00	0.03	0.18	0.02
Al_2O_3	22.23	22.28	21.32	21.37	21.90	22.03	22.48	22.33	21.78	21.93	22.01	21.74	20.56	22.15	22.32	21.28	22.25
Cr_2O_3	0.05	0.06	0.01	0.06	0.01	0.01	0.05	0.01	0.14	0.27	0.19	0.05	1.45	0.03	0.04	0.95	0.02
FeO[a]	23.81	24.65	23.93	25.21	24.36	24.46	24.97	24.67	22.66	22.32	22.23	23.65	25.52	25.02	24.93	21.54	23.67
MnO	0.59	0.64	1.37	1.61	2.22	0.79	0.50	0.35	0.43	0.50	0.41	0.35	0.23	0.63	0.54	0.39	0.49
MgO	9.49	9.64	7.48	6.93	7.00	8.27	9.51	9.60	7.21	8.16	7.43	4.84	4.48	9.70	9.55	7.31	9.18
CaO	4.49	4.00	6.57	6.54	6.20	5.83	3.73	4.18	9.02	7.87	9.17	10.60	9.22	3.63	3.69	8.29	5.22
Total	100.19	100.85	99.38	100.61	100.55	100.73	100.50	100.11	100.72	100.93	100.66	100.27	98.92	100.65	100.32	98.87	100.86
Si	3.01	2.99	2.99	2.99	2.98	2.99	2.98	2.97	3.00	2.99	2.98	3.02	2.96	2.99	2.98	3.02	3.02
Al	1.99	1.99	1.95	1.94	1.98	1.97	2.01	2.00	1.95	1.96	1.97	1.98	1.91	1.98	2.00	1.95	1.98
Ti	0.00	0.00	0.00	0.00	0.00	0.00	0.00	0.00	0.00	0.03	0.00	0.00	0.00	0.00	0.00	0.01	0.00
Cr	0.00	0.00	0.00	0.00	0.00	0.00	0.00	0.00	0.01	0.02	0.01	0.00	0.09	0.00	0.00	0.06	0.00
Fe^{3+}	0.00	0.03	0.07	0.09	0.05	0.05	0.04	0.07	0.03	0.01	0.06	0.00	0.12	0.05	0.04	0.00	0.00
Mg	1.08	1.09	0.86	0.79	0.80	0.94	1.08	1.09	0.82	0.92	0.84	0.56	0.53	1.10	1.08	0.85	1.03
Fe^{2+}	1.51	1.53	1.48	1.53	1.52	1.51	1.55	1.50	1.42	1.40	1.35	1.53	1.56	1.54	1.54	1.40	1.49
Mn	0.04	0.04	0.09	0.10	0.14	0.05	0.03	0.02	0.03	0.03	0.03	0.02	0.02	0.04	0.03	0.03	0.03
Ca	0.37	0.32	0.55	0.54	0.51	0.48	0.30	0.34	0.74	0.64	0.75	0.88	0.78	0.29	0.30	0.69	0.42
Uvarovit	0.15	0.18	0.03	0.18	0.03	0.03	0.14	0.03	0.43	0.82	0.56	0.16	4.27	0.09	0.13	2.90	0.05
Andradit	0.00	1.49	3.59	4.29	2.33	2.23	1.82	3.23	1.35	0.45	3.02	0.00	5.70	2.24	1.96	0.00	0.00
Pyrop	35.93	36.46	29.02	26.73	26.96	31.53	36.38	36.86	27.30	30.75	28.40	18.67	18.27	36.88	36.54	28.59	34.65
Spessartin	1.27	1.38	3.02	3.53	4.86	1.71	1.08	0.76	0.92	1.07	0.88	0.77	0.53	1.36	1.17	0.86	1.05
Almandin	50.58	51.29	49.64	51.62	51.03	50.79	52.29	50.85	47.23	46.87	45.55	51.16	54.18	51.84	52.14	47.25	50.14
Grossular	12.07	9.21	14.70	13.66	14.80	13.71	8.30	8.28	22.76	20.04	21.60	29.23	17.06	7.59	8.06	20.40	14.11

[a]Total iron. Calculation on the basis of Grt = 12 oxygens

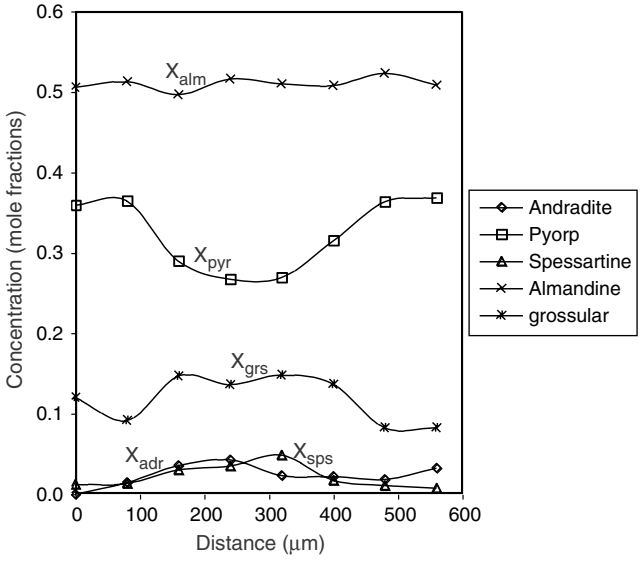

Fig. 6 Garnet compositional profile in the eclogite from the Huangzhen-Zhujiachong area in South Dabie. The zonation indicates a prograde metamorphic process

ture. Occasionally white mica (97H15) also occurs in the veins. Omphacite is also replaced by symplectites in variable degrees. The boundaries of quartz grains are usually straight, but sutured boundaries of quartz are also well developed in some samples (97H01, 97H02, 97H05 and 97H06). Quartzes show little undulose extinction and kink-bands, and rare fractures.

Amphibolite and gneiss

Amphibolite resulted from retrogression of previous eclogites, and is made up of elongated garnet, aligned hornblende, plagioclase and quartz. Accessories are muscovite, biotite, clinozoisite, and rutile.

Gneiss represents the country rock of host eclogite and veins, and is composed of quartz, biotite, plagioclase, sometimes garnet, epidote group minerals, apatite and rare magnetite. The foliation is defined by oriented mica flakes and elongated plagioclase.

Mineral chemistry

The microprobe analysis was systematically carried out on minerals that are present in host eclogites and veins. The results are listed in Tables 2 and 3.

Garnet grain in the eclogite shows a zonation from core to margin (Table 2 and Fig. 6). Pyrope increases ($Pyp_{26.73}$ to $Pyp_{36.86}$), while grossular shows a slight decrease from core to margin ($Grs_{14.80}$ to $Grs_{8.28}$), corresponding to a process of progressive metamorphism.

Table 3 Chemical composition of representative minerals in quartz segregations and eclogites at Huangzheng in South Dabie

	97H59-11	97H59-21	97H05-2	97H01-3	97H59-11in	97H59-12	97H05-1	97H05-2	97H59-12	97H59-61	97H59-62	97H59-63	97H02-2	97H59-63	97H01-2	97H02-1	97H02-12
	Minerals in eclogite									Minerals in vein							
	Omphacite				Amphibole				plagioclase	Omphacite				Amphibole			Plagioclase
SiO_2	55.80	54.88	55.99	57.29	46.48	38.83	51.35	52.12	64.31	55.75	55.98	56.14	55.91	42.40	54.42	52.13	49.81
TiO_2	0.07	0.00	0.03	0.04	0.02	0.02	0.10	0.09	0.00	0.00	0.00	0.03	0.01	0.02	0.057	0.079	0.124
Al_2O_3	9.41	10.29	10.33	11.5	14.02	18.38	8.07	7.99	22.05	9.75	10.12	10.24	10.07	16.60	5.76	8.98	9.22
Cr_2O_3	0.01	0.07	0.04	0.039	0.28	0.03	1.88	1.00	0.10	0.04	0.03	0.08	0.04	0.07	0.049	0.173	2.79
FeO	8.32	7.69	6.88	3.38	10.46	14.70	6.73	6.77	0.21	7.56	8.11	8.36	7.52	12.72	4.72	7.84	7.74
MnO	0.02	0.00	0.01	0	0.06	0.16	0.04	0.05	0.00	0.06	0.00	0.10	0.02	0.11	0.033	0.075	0.036
MgO	6.85	6.93	7.32	8.44	13.35	10.70	16.78	16.79	0.04	7.11	7.07	7.11	7.17	11.74	19.15	15.61	15.6
CaO	10.35	10.13	10.82	12.43	7.79	10.70	7.31	7.35	3.33	10.81	10.35	10.17	10.66	9.48	9.28	6.44	6.32
Na_2O	8.67	8.70	8.33	7.42	4.53	3.57	4.46	4.60	9.77	8.42	8.54	8.63	8.43	3.99	3.46	5.37	4.96
K_2O	0.02	0.01	0.01	0	0.34	0.68	0.20	0.19	0.08	0.00	0.01	0.00	0.01	0.29	0.171	0.191	0.213
NiO	0.00	0.00	0.03	0.084	0.00	0.00	0.11	0.11	0.03	0.00	0.02	0.05	0.02	0.00	0.216	0.039	0.064
Total	99.52	98.70	99.77	100.62	97.33	97.76	97.02	97.04	99.92	99.50	100.23	100.91	99.84	97.41	97.317	96.927	96.876
Oxygen	6.00	6.00	6.00	6.00	23.00	23.00	23.00		8.00	6.00	6.00	6.00	6.00	23.00	23.00	23.00	23.00
Si	1.99	1.97	1.99	2.01	6.69	5.80	7.27	7.35	2.84	1.99	1.98	1.98	1.99	6.22	7.57	7.37	7.12
Al	0.40	0.43	0.43	0.48	2.38	3.24	1.35	1.33	1.15	0.41	0.42	0.43	0.42	2.87	0.94	1.50	1.55
Ti	0.00	0.00	0.00	0.00	0.00	0.00	0.01	0.01	0.00	0.00	0.00	0.00	0.00	0.00	0.01	0.01	0.01
Cr	0.00	0.00	0.00	0.00	0.03	0.00	0.21	0.11	0.00	0.00	0.00	0.00	0.00	0.01	0.01	0.02	0.32
Fe^{3+}	0.00	0.00	0.00	0.00	0.00	0.00	0.00	0.00	0.01	0.00	0.00	0.00	0.00	0.00			
Fe^{2+}	0.25	0.23	0.20	0.10	1.26	1.84	0.80	0.80	0.00	0.23	0.24	0.25	0.22	1.56	0.55	0.93	0.92
Mn	0.00	0.00	0.00	0.00	0.01	0.02	0.00	0.01	0.00	0.00	0.00	0.00	0.00	0.01	0.00	0.01	0.00
Mg	0.37	0.37	0.39	0.44	2.87	2.38	3.54	3.53	0.00	0.38	0.37	0.37	0.38	2.56	3.97	3.29	3.32
Ca	0.40	0.39	0.41	0.47	1.20	1.71	1.11	1.11	0.16	0.41	0.39	0.38	0.41	1.49	1.38	0.98	0.97
Na	0.60	0.61	0.57	0.50	1.26	1.03	1.23	1.26	0.84	0.58	0.59	0.59	0.58	1.14	0.93	1.47	1.37
K	0.00	0.00	0.00	0.00	0.06	0.13	0.04	0.03	0.00	0.00	0.00	0.00	0.00	0.06	0.03	0.03	0.04
Ni	0.00	0.00	0.00	0.00	0.00	0.00	0.01	0.01	0.00	0.00	0.00	0.00	0.00	0.00	0.02	0.00	0.01
WEF	45.68	45.01	46.75	50.13						46.65	46.16	46.07	46.52				
JD	54.32	54.99	53.25	49.87						53.35	53.84	53.93	53.48				
AE	0.00	0.00	0.00	0.00						0.00	0.00	0.00	0.00				
An									15.87								
Ab									84.13								
ps																	

Garnet in the vein exhibits no zonation, but is chemically consistent with the margin of garnets in host eclogite (Table 2). Most garnets in both eclogites and veins contain a clear retrograde rim of amphibole in chemical composition.

Omphacite mostly shows the strong retrogressive symplectite texture of mixing amphibole and plagioclase, and usually has a homogeneous chemical composition from core to rim. The jadeite content in the omphacite falls in the range of 49–55%.

Amphibole is present in both eclogites and veins, and in different textures and variable compositions (Table 3). Most of the amphiboles occur as the retrogressive symplectite of omphacite and the rim of garnet, containing MgO of 10.70–19.15% and Na_2O of 3.46–5.37%. Occasionally, amphibole gets included in the garnet of eclogite, pointing to its formation before peak metamorphic conditions. There is no obvious difference for the amphiboles in chemical composition between host eclogites and veins.

Zoisite/clinozoisite has two generations, but they have relative homogeneous chemical composition with pistacite components of 12–16% and Fe^{3+} ranging from 0.35 to 0.42 atoms pfu. The early generation with coarse-grain size probably formed prior to the peak metamorphic conditions, while the later one with fine-grain size may partially result from the breakdown of lawsonite into the mineral assemblage of kyanite, zoisite/clinozoisite and quartz.

Kyanite occurs not only in the quartz–kyanite vein, but also is found as inclusions within the omphacite of host eclogite. This indicates two generations of kyanite that resulted from mostly retrograde and occasionally prograde processes, respectively. Analyzed kyanite contains up to 0.08∼0.29% Cr_2O_3 and 0.32∼0.43% FeO in the composition.

Plagioclase is of retrograde origin and was absent from the peak eclogite assemblage. The plagioclase formed by replacement reactions that occurred in the textural settings of intergrowth with amphibole in symplectites after omphacite and in fine-grained symplectites after kyanite. The chemical composition varies greatly from An_{11} to An_{36}.

Paragonite exists pervasively in both eclogites and veins, with Na content up to 1.63∼1.90 and K content of 0.05∼0.13 atom pfu (Table 3). Talc has also been found in the quartz veins.

Estimate of *P–T* conditions

The textural relationship and the mineral composition data indicate that the initial UHP and plagioclase-free assemblage was garnet + omphacite + kyanite +

97H59-61	97H02-1	97H59-52	97H59-12	97H59-21	97H05-1	97H59-2	97H05-2	97H59-61	97H02-1	97H59-61	97H59-62	97H02-1	97H01-2	97H01-31	97H01-32	97H01-33	97H02-1	97H02-2
		Minerals in eclogite						Minerals in vein										
		Clinozoisite			kyanite	Paragonite		Clinozoisite		Kyanite			Paragonite					
65.39	59.69	38.44	38.30	38.90	38.32	47.38	47.58	38.54	38.83	37.58	38.42	37.53	47.22	47.79	47.14	46.94	46.94	47.08
0.00	0	0.15	0.09	0.06	0.00	0.04	0.08	0.02	0.07	0.00	0.02	0.00	0.04	0.02	0.00	0.02	0.05	0.05
21.34	25.55	28.58	27.95	29.59	62.66	40.58	38.66	28.95	29.45	62.29	60.96	61.99	38.72	38.99	38.83	38.64	38.58	38.96
0.10	0	0.00	0.00	0.00	0.12	0.37	0.08	0.00	0.00	0.08	0.29	0.06	0.05	0.18	0.03	0.42	0.06	0.07
0.21	0.145	6.45	6.78	5.42	0.43	0.76	0.44	5.93	5.57	0.32	0.42	0.42	0.28	0.46	0.38	0.36	0.27	0.38
0.00	0	0.02	0.01	0.00	0.02	0.00	0.00	0.00	0.00	0.02	0.00	0.02	0.04	0.00	0.01	0.01	0.00	0.00
0.04	0	0.20	0.13	0.22	0.01	0.23	0.26	0.28	0.22	0.01	0.01	0.02	0.23	0.21	0.17	0.15	0.22	0.12
2.36	7.42	23.14	23.82	23.27	0.05	0.27	0.30	23.13	23.25	0.03	0.07	0.04	0.36	0.32	0.27	0.47	0.33	0.32
9.93	7.14	0.06	0.03	0.01	0.07	6.69	7.18	0.03	0.02	0.02	0.13	0.06	7.26	6.80	7.05	7.01	7.24	6.85
0.08	0.06	0.01	0.02	0.00	0.03	0.84	1.01	0.02	0.00	0.00	0.00	0.04	0.80	0.86	0.82	0.59	0.78	0.83
0.03	0	0.03	0.03	0.04	0.01	0.00	0.04	0.03	0.04	0.00	0.05	0.00	0.00	0.00	0.04	0.00	0.00	0.06
99.47	100.01	97.08	97.16	97.50	101.73	95.16	95.63	96.93	97.44	100.35	100.37	100.18	95.00	95.63	94.74	94.61	94.47	94.73
8.00	8.00	12.50	12.50	12.50	5.08	22.00	22.00	12.5	12.5	5	5	5	22	22	22	22	22	22
2.89	2.66	3.01	2.98	3.01	1.03	5.95	6.07	3.01	3.01	1.01	1.03	1.01	6.06	6.08	6.06	6.04	6.05	6.05
1.11	1.34	2.63	2.56	2.70	1.99	6.00	5.81	2.66	2.69	1.98	1.94	1.97	5.85	5.85	5.88	5.86	5.86	5.90
0.00	0.00	0.01	0.01	0.00	0.00	0.00	0.01	0.00	0.00	0.00	0.00	0.00	0.00	0.00	0.00	0.00	0.00	0.00
0.00	0.00	0.00	0.00	0.00	0.00	0.04	0.01	0.00	0.00	0.00	0.01	0.00	0.00	0.02	0.00	0.04	0.01	0.01
0.01	0.00	0.42	0.47	0.35				0.39	0.36									
0.00	0.01	0.00	0.00	0.00	0.01	0.08	0.05	0.00	0.00	0.01	0.01	0.00	0.03	0.05	0.04	0.04	0.03	0.04
0.00	0.00	0.00	0.00	0.00	0.00	0.00	0.00	0.00	0.00	0.00	0.00	0.00	0.00	0.00	0.00	0.00	0.00	0.00
0.00	0.00	0.02	0.02	0.03	0.00	0.04	0.05	0.03	0.03	0.00	0.00	0.00	0.04	0.04	0.03	0.03	0.04	0.02
0.11	0.35	1.93	1.99	1.93	0.00	0.04	0.04	1.93	1.93	0.00	0.00	0.00	0.05	0.04	0.04	0.07	0.04	0.04
0.85	0.62	0.01	0.00	0.00	0.00	1.63	1.78	0.00	0.00	0.00	0.01	0.00	1.81	1.68	1.76	1.75	1.81	1.71
0.00	0.00	0.00	0.00	0.00	0.00	0.13	0.16	0.00	0.00	0.00	0.00	0.00	0.13	0.14	0.13	0.10	0.13	0.14
0.00	0.00	0.00	0.00	0.00	0.00	0.00	0.00	0.00	0.00	0.00	0.00	0.00	0.00	0.00	0.00	0.00	0.00	0.01
11.61	36.48																	
88.39	63.52																	
		0.14	0.67	0.12				0.13	0.12									

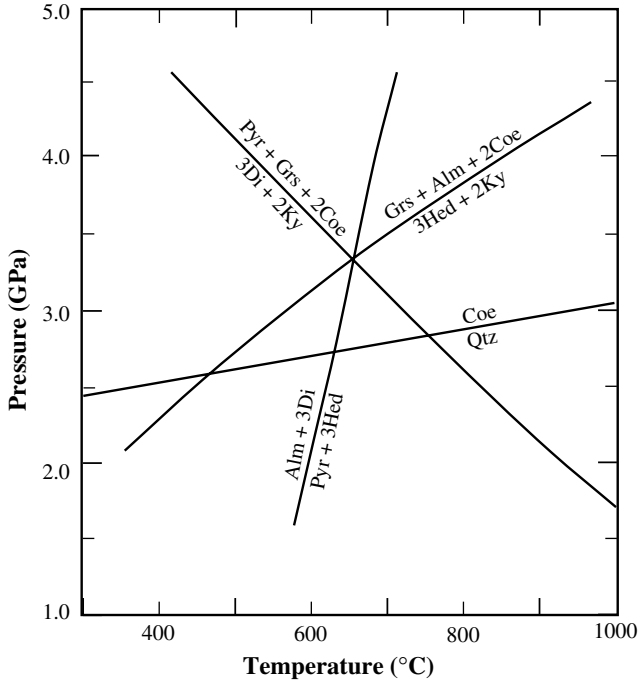

Fig. 7 Estimates of peak metamorphic condition for the eclogite and vein samples from the Huangzhen-Zhujiachong area in South Dabie using thermocalc and calibrated reactions

lawsonite + clinozoisite + rutile + coesite. The well-developed prograde zonation pattern is observed with an increase in pyrope and a decrease in grossular and spessartine contents from core to rim (Fig. 6). This implies that garnet cores formed under relatively low *P–T* conditions, whereas rims formed under higher *P–T* conditions.

Since the pseudomorphs of coesite are found in the investigated samples (Fig. 3), peak *P–T* conditions are constrained by the occurrence of coesite and by the coexistence of unzoned omphacite in equilibrium with end-member kyanite as well as by the chemical composition of garnet rim and three net-transfer equilibria (Terry et al. 2000). Following the THERMOCALC method of Powell and Holland (1988) with the internally-consistent database of Holland and Powell (1998), and the garnet and clinopyroxene activity model of Holland and Powell (1990), peak metamorphic *P–T* conditions are calculated to be at about 670°C and 3.3 GPa (Fig. 7). This is illustrated in Fig. 8a as point C in comparison with the literature data (dotted curves). Apparently, the calculated peak *P–T* conditions are significantly higher in comparison to the other studies (Wang et al. 1993; Okay et al. 1993), but consistent with the occurrence of coesite and the compositions of garnet and omphacite in the investigated samples.

The *P–T* conditions in the host eclogite of point A in Fig. 8a are taken from the previous study of the "cold" eclogite by Okay (1993). A possible reaction involved in the prograde metamorphic processes is paragonite = omphacite + kyanite + H_2O (Fig. 8a) although kyanite could also form after plagioclase breakdown during prograde metamorphism. It is clearly observed from our petrological investigation that paragonite was replaced by omphacite + kyanite assemblage at high-P

Fig. 8 *P–T* constrains on **a** eclogite and **b** kyanite–quartz vein from the Huangzhen-Zhujiachong area in South Dabie. *Dashed curves* denote the previous estimates of *P–T* paths. *P–T* boundaries of various subdivisions of the eclogite field including blueschist, amphibolite eclogite, epidote eclogite, lawsonite eclogite and dry eclogite are from Okamoto and Maruyama (1999)

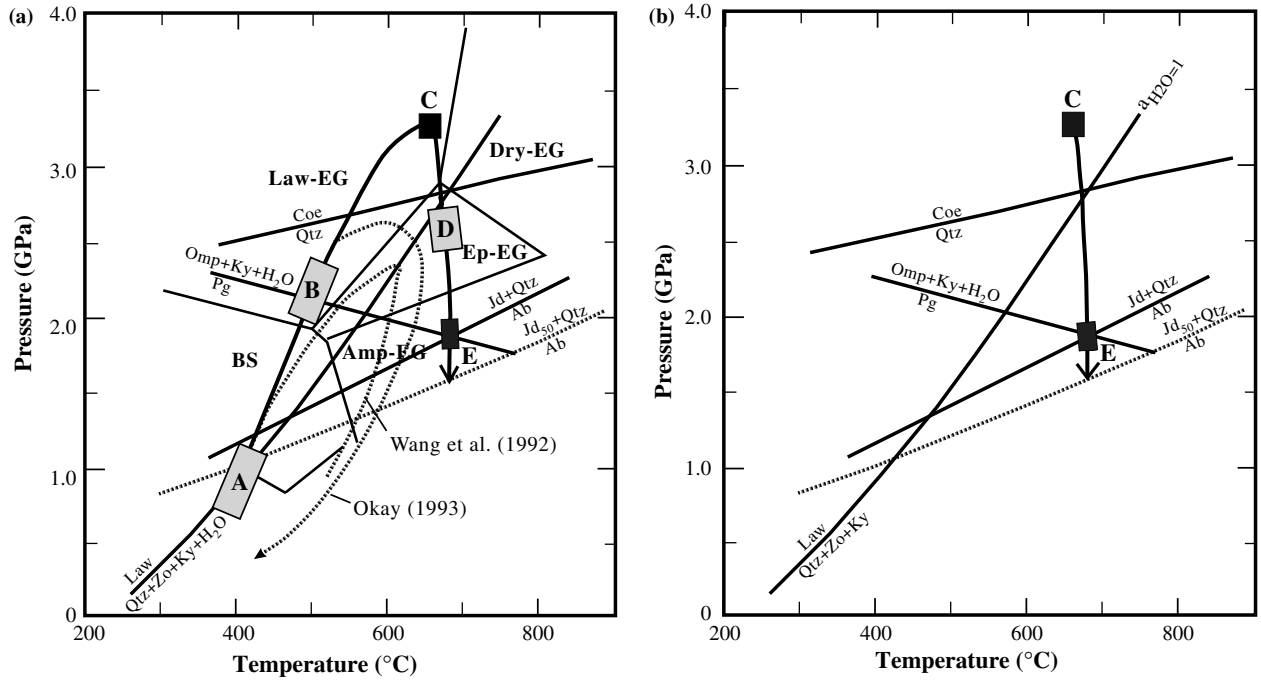

Table 4 SHRIMP U–Pb data for zircons from eclogite 97H05 in South Dabie

Spot	U (ppm)	Th (ppm)	Th/U	Pb_c (%)	$^{206}Pb^*$ (ppm)	$^{207}Pb^*/^{206}Pb^*$	± (%)	$^{207}Pb^*/^{235}U$	± (%)	$^{206}Pb^*/^{238}U$	± (%)	$^{206}Pb/^{238}U$ Age (Ma)	$^{207}Pb/^{206}Pb$ Age (Ma)
1.1	1,643	23	0.01	0.87	54.9	0.04385	7.6	0.233	7.8	0.03854	2.0	244 ± 5	
1.2	832	20	0.02	0.87	27.6	0.05263	5.5	0.278	5.8	0.03831	2.0	242 ± 5	313 ± 125
2.1	325	198	0.61	0.17	46.3	0.10118	13.3	2.312	14.2	0.16572	2.1	988 ± 22	1,646 ± 247
2.2	767	13	0.02	1.61	25.9	0.04302	6.2	0.229	6.2	0.03861	2.1	244 ± 5	
3.1	1,282	24	0.02	0.27	42.4	0.04608	8.5	0.244	8.7	0.03840	2.0	243 ± 5	2 ± 205
4.1	219	105	0.48	0.26	45.3	0.10583	9.5	3.498	9.8	0.23972	2.2	1,385 ± 34	1,729 ± 174
5.1	255	70	0.27	1.24	12.4	0.07806	31.6	0.601	31.1	0.05584	2.3	350 ± 8	1,148 ± 628
6.1	1,427	13	0.01	0.47	46.3	0.04587	27.8	0.238	28.7	0.03763	2.0	238 ± 5	
6.2	259	3	0.01	3.25	8.02	0.04977	22.6	0.239	22.5	0.03483	3.3	221 ± 7	184 ± 526
7.1	1,134	22	0.02	0.10	34.3	0.04983	18.2	0.242	18.6	0.03522	2.2	223 ± 5	187 ± 424
7.2	317	161	0.51	0.23	41.9	0.09531	26.6	2.016	26.5	0.15341	2.9	920 ± 29	1,534 ± 501
8.1	771	5	0.01	0.86	26.1	0.04763	12.9	0.257	12.5	0.03913	2.2	247 ± 6	
9.1	1,186	15	0.01	0.52	38.3	0.04174	41.3	0.215	41.5	0.03736	2.0	236 ± 5	
9.2	145	56	0.38	0.75	30.0	0.11303	19.3	3.722	18.5	0.23882	2.4	1,381 ± 37	1,849 ± 349
10.1	884	20	0.02	0.87	29.9	0.04486	15.2	0.241	14.5	0.03896	2.1	246 ± 5	
11.1	696	11	0.01	1.67	21.2	0.04981	20.3	0.241	20.2	0.03503	2.2	222 ± 6	186 ± 470

Note Pb_c and Pb* denote the common and radiogenic portions, respectively

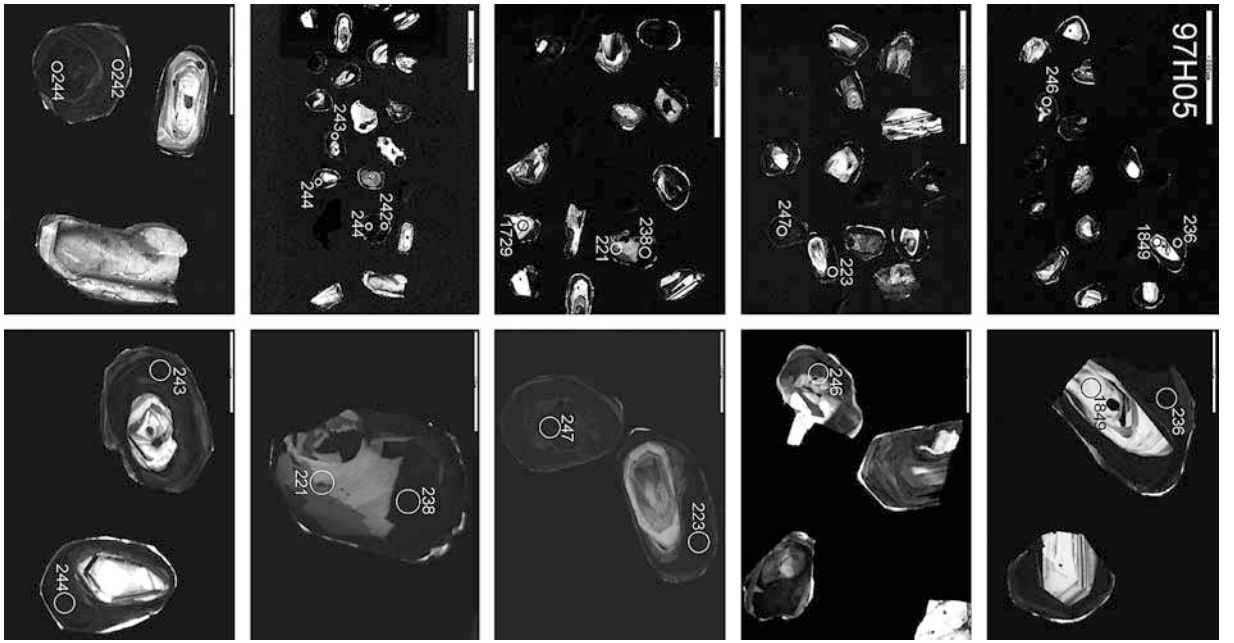

Fig. 9 CL images of zircon grains with the SHRIMP U–Pb age for eclogite 97H05 from the Huangzhen-Zhujiachong area in South Dabie

conditions as a stable assemblage in the eclogites. Nevertheless, the preservation of relict paragonite in kyanite and omphacite means that the eclogite would at least pass over the reaction paragonite = kyanite + omphacite + H_2O during subduction, and experienced metamorphism at point B of the *P*–*T* path in Fig. 8a with pressures greater than 2.0 GPa.

Peak *P*–*T* conditions can also be figured out for the veins of eclogite (Fig. 8b). Calculation was carried out by using the measured unzoned composition of garnet, neighboring unzoned omphacite and end-member kyanite as input data. Since the composition of garnet in the veins is similar to that in the rim of garnet in the host eclogite, no significant difference in peak *P*–*T* values is

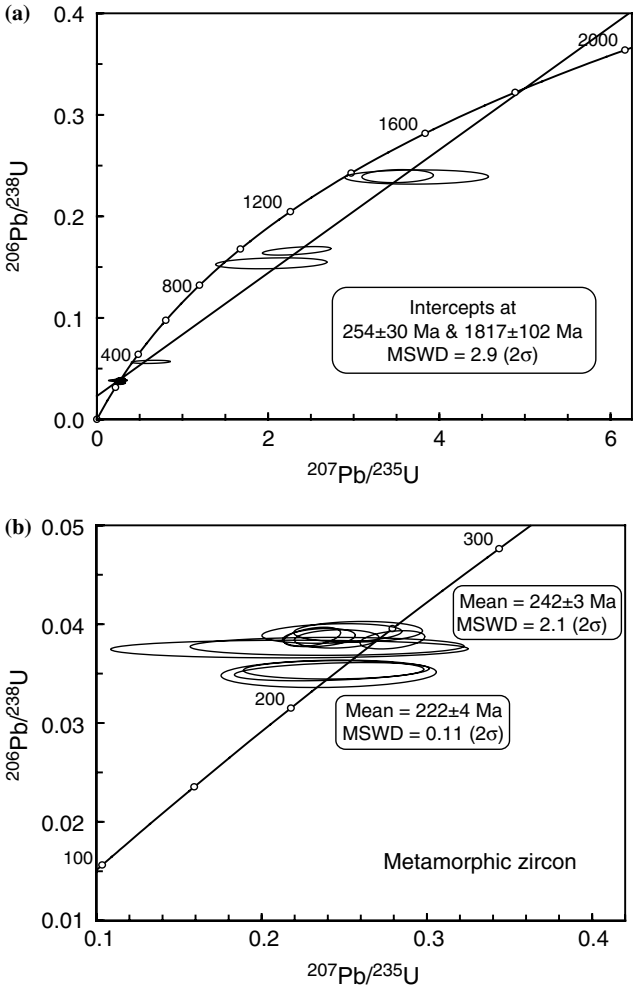

Fig. 10 Zircon SHRIMP U–Pb dating for eclogite 97H05 from the Huangzhen-Zhujiachong area in South Dabie. **a** All data are regressed to yield a discordia line with $t_1 = 1{,}817 \pm 102$ Ma and $t_2 = 254 \pm 30$ Ma. **b** Triassic $^{206}Pb/^{238}U$ spot-ages are categorized into two groups at 242 ± 3 Ma and 222 ± 4 Ma, respectively

obtained with respect to the host eclogite (Fig. 8a). Thus peak *P–T* conditions for vein formation are also at about 670°C and 3.3 GPa (Fig. 8b). Upon decompression subsequent to peak UHP conditions, lawsonite is expected to decompose at about 2.5 GPa when across its stable reaction line at point D along the *P–T* path (Fig. 8a), resulting in the formation of kyanite + clinozoisite + coesite assemblage with H_2O release in the infancy of exhumation. The ideal activity model for clinozoisite is used to calculate the reaction proposed by Holland and Powell (1998). Upon decompression decomposition, garnet and omphacite were retrograded to produce plagioclase and amphibole, respectively, releasing CaO and Na_2O. The released CaO and Na_2O components were diffused into the domains between kyanite and quartz grains to react, producing plagioclase between them (Nakamura 2002).

Point E in both Fig. 8a and b denotes the *P–T* conditions under which garnet was overgrown by retrograde sodic amphibole rim, omphacite brokedown into

Table 5 Sm–Nd and Rb–Sr isotope compositions of eclogite minerals and whole-rock in South Dabie

Sample no.	Sm (ppm)	Nd (ppm)	$^{147}Sm/^{144}Nd$	$^{143}Nd/^{144}Nd$	$\varepsilon_{Nd}(t_2)$ 230 Ma	$\varepsilon_{Nd}(t_1)$ 1,800 Ma	T_{DM} (Ga)	Rb (ppm)	Sr (ppm)	$^{87}Rb/^{86}Sr$	$^{87}Sr/^{86}Sr$	$I_{Sr}(t_2)$ 230 Ma	$I_{Sr}(t_1)$ 1,800 Ma
97H05 Mineral													
Kyanite	2.079	4.826	0.2604	0.512269	−9.1			2.214	218.5	0.029	0.706084	0.70599	
Omphacite	0.898	4.443	0.1222	0.512096	−8.4			0.483	111.7	0.013	0.706164	0.70612	
Paragonite								28.65	51.84	1.600	0.711295	0.70606	
Garnet	0.934	0.285	1.9838	0.514940	−7.5								
Rutile	0.030	0.154	0.1193	0.512033	−9.5								
Whole-rock													
97H02	6.91	33.46	0.1248	0.512034 ± 7	−9.7	4.9	1907	13.13	366.8	0.028	0.705437 ± 8	0.70535	0.70470
97H06	5.48	25.65	0.1293	0.512074 ± 9	−9.0	4.7	1936	16.32	443.2	0.089	0.706388 ± 10	0.70610	0.70406
97H14	4.54	21.65	0.1269	0.512113 ± 11	−8.2	6.0	1816	25.27	336.7	0.067	0.706592 ± 7	0.70637	0.70484
97H30	5.75	25.56	0.1359	0.512203 ± 5	−6.7	5.6	1850	12.43	293.6	0.052	0.705902 ± 9	0.70573	0.70454
97H32	4.33	21.83	0.1200	0.512004 ± 8	−10.1	5.4	1859	19.54	421.5	0.064	0.706271 ± 8	0.70606	0.70460
97H51	5.24	23.79	0.1331	0.512168 ± 13	−7.3	5.6	1852	21.65	387.3	0.076	0.706033 ± 10	0.70578	0.70404

Note initial Nd and Sr isotope ratios $\varepsilon_{Nd}(t_1)$ and $\varepsilon_{Nd}(t_2)$ as well as $I_{Sr}(t_1)$ and $I_{Sr}(t_2)$ are calculated at $t_1 = 1{,}800$ Ma and $t_2 = 230$ Ma, respectively; Nd model age T_{DM} is calculated using a single-stage model relative to the depleted mantle

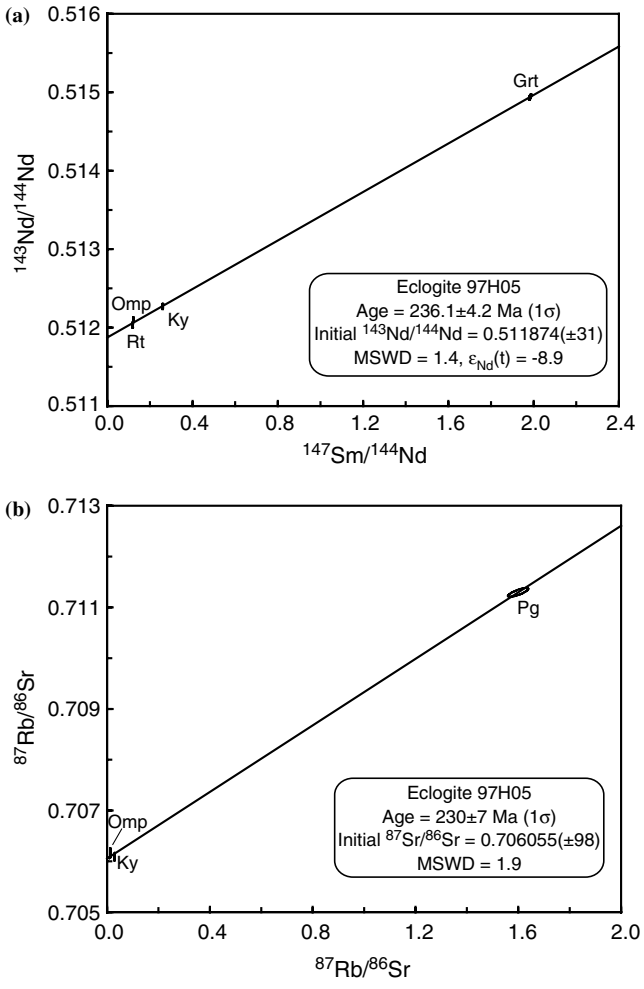

Fig. 11 Mineral Sm–Nd and Rb–Sr isochron dating on eclogite 97H05 from the Huangzhen-Zhujiachong area in South Dabie

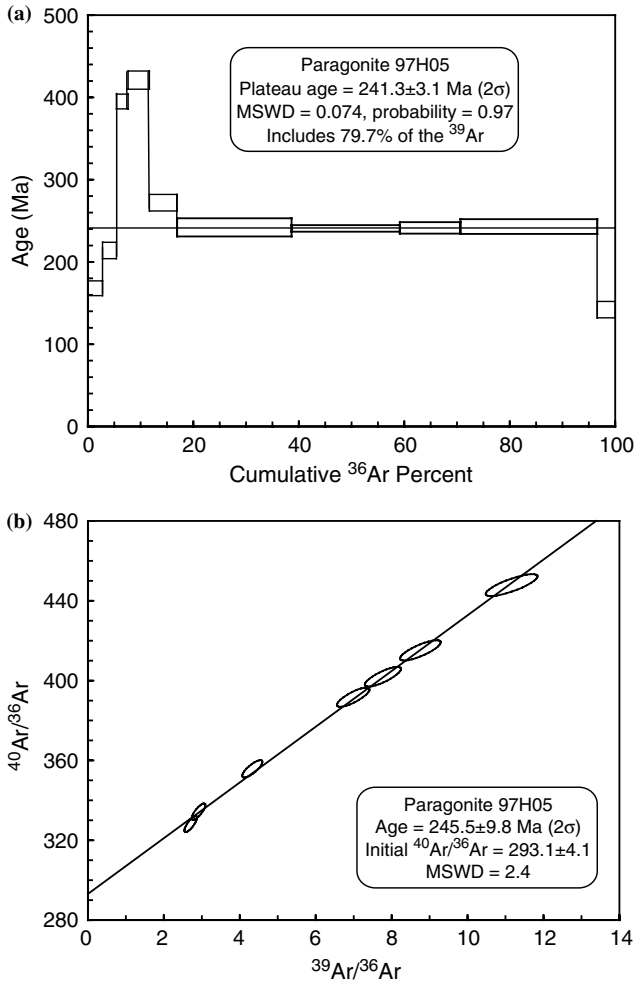

Fig. 12 Paragonite Ar–Ar dating on eclogite 97H05 from the Huangzhen-Zhujiachong area in South Dabie

amphibole and plagioclase, kyanite was also rimed by plagioclase between the contact of quartz and kyanite (Fig. 4f). The mineral assemblage of Grt–Omp–Prg–Fsp–Ky–Qtz, therefore, well represents the retrograde stage from epidote eclogite to amphibole eclogite. The average *P–T* conditions of point E were also calculated using the THERMOCALC method from all linearly independent reactions for the coexisted real mineral compositions of garnet, omphacite, pargasite, feldspar, end-member kyanite and quartz and water, which rep-

Table 6 Ar–Ar isotope data on paragonite in eclogite 97H05 from South Dabie

T (°C)	$(^{40}Ar/^{39}Ar)_m$	$(^{36}Ar/^{39}Ar)_m$	$(^{37}Ar/^{39}Ar)_m$	$(^{38}Ar/^{39}Ar)_m$	^{39}Ar (10^{-14} mol)	^{39}Ar (%)$_{cum}$	$^{40}Ar^*$	t (Ma)	±1σ (Ma)
600	114.7123	0.3431	0.1414	0.0110	16.64	2.79	9.3662	168.0	9.1
700	121.1745	0.3693	0.2474	0.0851	15.63	5.41	12.0586	214.0	10.2
800	104.3556	0.2738	0.1095	0.0804	10.14	6.71	23.4487	395.0	9.6
900	65.5477	0.1367	0.0716	0.0496	29.52	11.66	23.1451	421.0	11.4
950	40.1275	0.0896	0.0176	0.0357	20.81	14.34	15.5724	272.0	10.3
1,000	56.0481	0.1431	0.0631	0.0399	144.87	38.63	13.7645	242.0	11.6
1,050	47.4085	0.1142	0.0597	0.0401	111.17	52.93	13.6768	240.8	4.2
1,150	51.7283	0.1287	0.0614	0.0400	105.57	70.63	13.7207	241.4	7.5
1,200	82.1510	0.2309	0.1595	0.0604	154.89	96.60	13.8155	243.0	9.7
1,300	84.8287	0.2607	0.5284	0.0859	20.28	100.00	7.8399	142.0	10.1

Notes T: step-heating temperature, $(^{40}Ar/^{39}Ar)_m$: measured ratio of ^{40}Ar to ^{39}Ar produced by irradiation of ^{39}K, $(^{36}Ar/^{39}Ar)_m$: measured ratio of corrected ^{36}Ar to ^{39}Ar, $(^{37}Ar/^{39}Ar)_m$ and $(^{38}Ar/^{39}Ar)_m$: measured ratios of corrected ^{37}Ar and ^{38}Ar to ^{39}Ar, ^{39}Ar: moles of ^{39}Ar corrected for blank, ^{39}Ar (%)cum: percentage of cumulative ^{39}Ar released, $^{40}Ar^*$: fraction of radiogenic, ^{40}Ar. Ar isotope ratios were corrected for blank and reactor-produced, ^{40}Ar; uncertainties for spectrum ages include 1% uncertainty in J factor (0.010443)

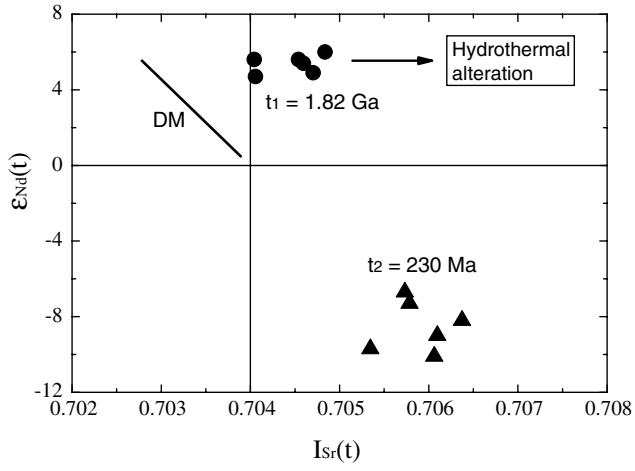

Fig. 13 Initial Nd and Sr isotope compositions of eclogite from the Huangzhen-Zhujiachong area in South Dabie, which are calculated at $t_2 = 230$ Ma and $t_1 = 1{,}800$ Ma, respectively

resent the reactions with retrograded mineral assemblage. The estimated *P–T* values of point E are 680°C and 1.8 GPa. Zhai et al. (1995) and Castelli et al. (1998) estimated the *P–T* conditions of 650–700°C and 1.8 GPa for peak metamorphism of the "cold" eclogite without coesite but with the presence of sodic amphiboles, similar to those for the amphibole eclogite from this study (Fig. 8). Since no albite is found in any of the investigated samples and omphacite contains about 49–54% jadeite end-member, the *P–T* path ends above the reaction Jd_{50} + Qtz = Ab (calibration based on Holland 1980).

Isotopic geochronology and geochemistry

Zircon U–Pb dating

Zircons were separated from an eclogite sample (97H05) for U–Pb dating by means of the SIMS technique, and the results are listed in Table 4. Zircons in this sample are mostly equant to short prismatic, colorless and transparent. The length of these grains ranges from 100 to 200 μm, with aspect ratios of 1:1–2:1. They are anhedral to subhedral. In CL imaging (Fig. 9), most of them show clear core-rim structures. Many of the cores display oscillatory zonation with moderate brightness, which is typical for magmatic zircon; a few of them display faint zoning that may be modified by solid-state recrystallization. The rims are unzoned or weakly zoned with weak luminescence. Core-rim boundaries are generally sharp and regular. It is clear from textural evidence that the rims represent overgrowth areas. Some grains are completely unzoned, weakly zoned or show fir-tree sector zoning, which may grow during metamorphism; a few of them show significant resorption around the core. Interaction of fluids with the cores in the course of rim overgrowth may explain these unusual internal structures.

The SHRIMP data on zircons from the eclogite yield two groups of Triassic $^{206}Pb/^{238}U$ spot-age (Fig. 10b) with consistently low Th/U ratios of 0.01–0.02 (Table 4): (1) seven spots at 236 ± 5 to 246 ± 5 Ma with a weighted mean of 243 ± 4 Ma (MSWD = 2.2), (2) three spots at 221 ± 7 to 223 ± 5 Ma with a weighted mean of 222 ± 4 Ma. Five spots of high Th/U ratios (0.27–0.61) correspond to $^{207}Pb/^{206}Pb$ ages of $1{,}148 \pm 628$ to $1{,}849 \pm 349$ Ma (Table 4) on inherited cores (Fig. 9) with a discordia upper-intercept age of $1{,}817 \pm 102$ Ma (Fig. 10a), indicating the variable preservation of magmatic cores during the eclogite-facies metamorphism. Because the nine spots of Triassic $^{206}Pb/^{238}U$ age have the very low Th/U ratios of 0.01–0.02, they are of metamorphic genesis with the equilibrium partition of Th and U when the zircon grew (and overgrew) during the eclogite-facies metamorphism (Hoskin 1998; Vavra et al. 1999). Therefore, the ages of 242 ± 3 and 222 ± 4 Ma dated the two metamorphic events that were recorded in the studied eclogite for subduction and exhumation of the Yangtze plate, respectively, during the Triassic collision.

Mineral Sm–Nd and Rb–Sr dating

Sm–Nd and Rb–Sr isotopic data for minerals from eclogite 97H05 are listed in Table 5. As depicted in Figure 11a, Sm–Nd isochron dating for garnet, kyanite, omphacite and rutile yields an age of 236.1 ± 4.2 Ma (MSWD = 1.4) with an initial $^{143}Nd/^{144}Nd$ ratio of $0.511874(\pm 31)$. The good isochron fitting indicates that Nd isotopic equilibrium was achieved among the minerals during the Triassic UHP metamorphism.

Figure 11b shows that Rb–Sr isochron dating for kyanite, omphacite and paragonite gives an age of 230 ± 7 Ma (MSWD = 1.9) with an initial $^{87}Sr/^{86}Sr$ ratio of $0.706055(\pm 98)$. The fitting of a reasonable isochron suggests that the involved minerals were formed at Sr isotopic equilibrium during the eclogite-facies metamorphism. Because of the very low $^{87}Rb/^{86}Sr$ ratios of kyanite and omphacite (Table 5), the slope of the Rb–Sr isochron is mainly defined by the data point of paragonite. The Rb–Sr isochron age of 230 ± 7 Ma is younger than, but similar to, the Sm–Nd isochron age of 236.1 ± 4.2 Ma within the analytical uncertainties. This indicates the attainment and preservation of Sm–Nd and Rb–Sr isotope equilibria between the eclogite minerals that were acquired during the Triassic eclogite-facies metamorphism.

Paragonite Ar–Ar dating

$^{40}Ar/^{39}Ar$ dating was carried out on paragonite from eclogite 97H05, and the results are listed in Table 6. Although apparent ages of ten steps at heating temperatures of 600–1,300°C are variable from 142 ± 10 to 421 ± 11 Ma, major steps including 79.7% of the ^{39}Ar release have relatively consistent ages of 241 ± 4 to 243 ± 9 Ma with a plateau age of 241.3 ± 3.1 Ma (Fig. 12a). A prominent increase in apparent age to

Table 7 Hydrogen and oxygen compositions of minerals in eclogites from the Huangzhen-Zhujiachong area and temperature estimates

Sample no.	Mineral	δD (‰)	$\delta^{18}O$ (‰)	Pair	$\Delta^{18}O$ (‰)	T (°C)[a]
97H02 Eclogite	Quartz		1.42			
	Paragonite	−77	−1.62	Qtz–Prg	3.04	515
	Omphacite		−1.46	Qtz–Omp	2.88	560
	Garnet		−2.38	Qtz–Grt	3.80	635
	Rutile		−6.04	Qtz–Rt	7.46	445
97H05e Eclogite	Quartz		−0.42			
	Paragonite	−81	−2.51	Qtz–Prg	2.22	680
	Kyanite		−2.61	Qtz–Ky	1.89	695
	Omphacite		−3.00	Qtz–Omp	2.26	690
	Zircon		−4.25	Qtz–Zr	3.43	685
	Garnet		−4.32	Qtz–Grt	3.50	680
	Rutile		−7.61	Qtz–Rt	6.69	495
97H06 Eclogite	Quartz		1.08			
	Paragonite	−87	−1.64	Qtz–Prg	2.72	570
	Omphacite		−0.84	Qtz–Omp	2.92	550
	Garnet		−2.76	Qtz–Grt	3.84	630
	Zoisite	−75	−2.16	Qtz–Czo	3.24	525
	Epidote	−68	−2.18	Qtz–Ep	3.26	515
	Rutile		−6.34	Qtz–Rt	7.42	450
97H14 Eclogite	Quartz		1.13			
	Paragonite	−85	1.78	Qtz–Prg	2.91	535
	Omphacite		−2.64	Qtz–Omp	3.77	425
	Garnet		−2.30	Qtz–Grt	3.43	690
	Rutile		−5.42	Qtz–Rt	6.55	505
97H30 Eclogite	Quartz		3.41			
	Kyanite		1.46	Qtz–Ky	1.95	680
	Paragonite	−78	0.58	Qtz–Prg	2.83	550
	Omphacite		−0.38	Qtz–Omp	3.79	425
	Garnet		−0.22	Qtz–Grt	3.63	660
	Epidote	−69	0.13	Qtz–Ep	3.28	515
97H32 Eclogite	Quartz		2.24			
	Paragonite	−83	−1.03	Qtz–Prg	3.27	480
	Omphacite		−0.51	Qtz–Omp	2.75	585
	Garnet		−1.43	Qtz–Grt	3.67	655
	Rutile		−5.28	Qtz–Rt	7.52	440
97H45c Eclogite	Quartz		3.42			
	Paragonite	−75	0.63	Qtz–Prg	2.79	560
	Amphibole	−73	−0.45	Qtz–Amp	3.17	555
	Omphacite		−0.54	Qtz–Omp	3.96	405
	Garnet		0.01	Qtz–Grt	3.41	695
	Zoisite	−66	−0.26	Qtz–Czo	3.68	465
	Rutile		−4.14	Qtz–Rt	7.56	440
97H51 Eclogite	Quartz		2.66			
	Kyanite		0.48	Qtz–Ky	2.18	620
	Paragonite	−83	−0.16	Qtz–Prg	2.50	615
	Omphacite		−1.22	Qtz–Omp	3.88	415
	Garnet		−1.02	Qtz–Grt	3.68	655
	Zoisite	−62	−0.19	Qtz–Czo	2.85	590
	Rutile		−4.49	Qtz–Rt	7.15	465
97H59 Eclogite	Quartz		1.67			
	Kyanite		−0.49	Qtz–Ky	2.16	625
	Paragonite	−79	−1.16	Qtz–Prg	2.83	550
	Omphacite		−2.08	Qtz–Omp	3.75	430
	Garnet		−2.01	Qtz–Grt	3.68	650
	Zoisite	−68	−1.34	Qtz–Czo	3.01	565
	Rutile		−6.02	Qtz–Rt	7.69	430
97H62 Eclogite	Quartz		4.41			
	Omphacite		1.82	Qtz–Omp	2.59	610
	Garnet		0.64	Qtz–Grt	3.77	640
	Rutile		−3.25	Qtz–Rt	7.66	435
97H18 Amphibolite	Quartz		9.87			
	Plagioclase		7.84	Qtz–Pl	2.03	395
	Muscovite	−85	6.86	Qtz–Mus	3.01	520
	Amphibole		6.35	Qtz–Hb	3.52	600
	Garnet		6.01	Qtz–Grt	3.86	625
	Biotite	−81	5.23	Qtz–Bt	4.64	490
	Rutile		2.35	Qtz–Rt	7.52	440

Table 7 (Contd.)

Sample no.	Mineral	δD (‰)	δ^{18}O (‰)	Pair	Δ^{18}O (‰)	T (°C)[a]
97H22b Amphibolite	Quartz		3.45			
	Plagioclase		1.38	Qtz–Pl	2.07	385
	Muscovite	−89	0.52	Qtz–Mus	2.93	535
	Amphibole	−85	−0.81	Qtz–Amp	4.26	505
	Garnet		−0.72	Qtz–Grt	4.17	585
	Biotite	−87	−1.24	Qtz–Bt	4.69	485
	Epidote	−54	−0.28	Qtz–Ep	3.73	455
97H23 Gneiss	Quartz		7.76			
	Plagioclase		6.01	Qtz–Pl	1.75	460
	Muscovite	−77	5.33	Qtz–Mus	2.43	630
	Magnetite		−0.54	Qtz–Mag	8.30	505
97H44 Gneiss	Quartz		2.84			
	Muscovite	−87	0.05	Qtz–Mus	2.79	555
	Garnet		−1.32	Qtz–Grt	4.16	585
	Biotite	−85	−1.87	Qtz–Bt	4.71	485
	Epidote	−61	−0.52	Qtz–Ep	3.36	500

[a]Temperaures were calculated using the fractionation factors calibrated by Zheng (1991, 1993a, b)

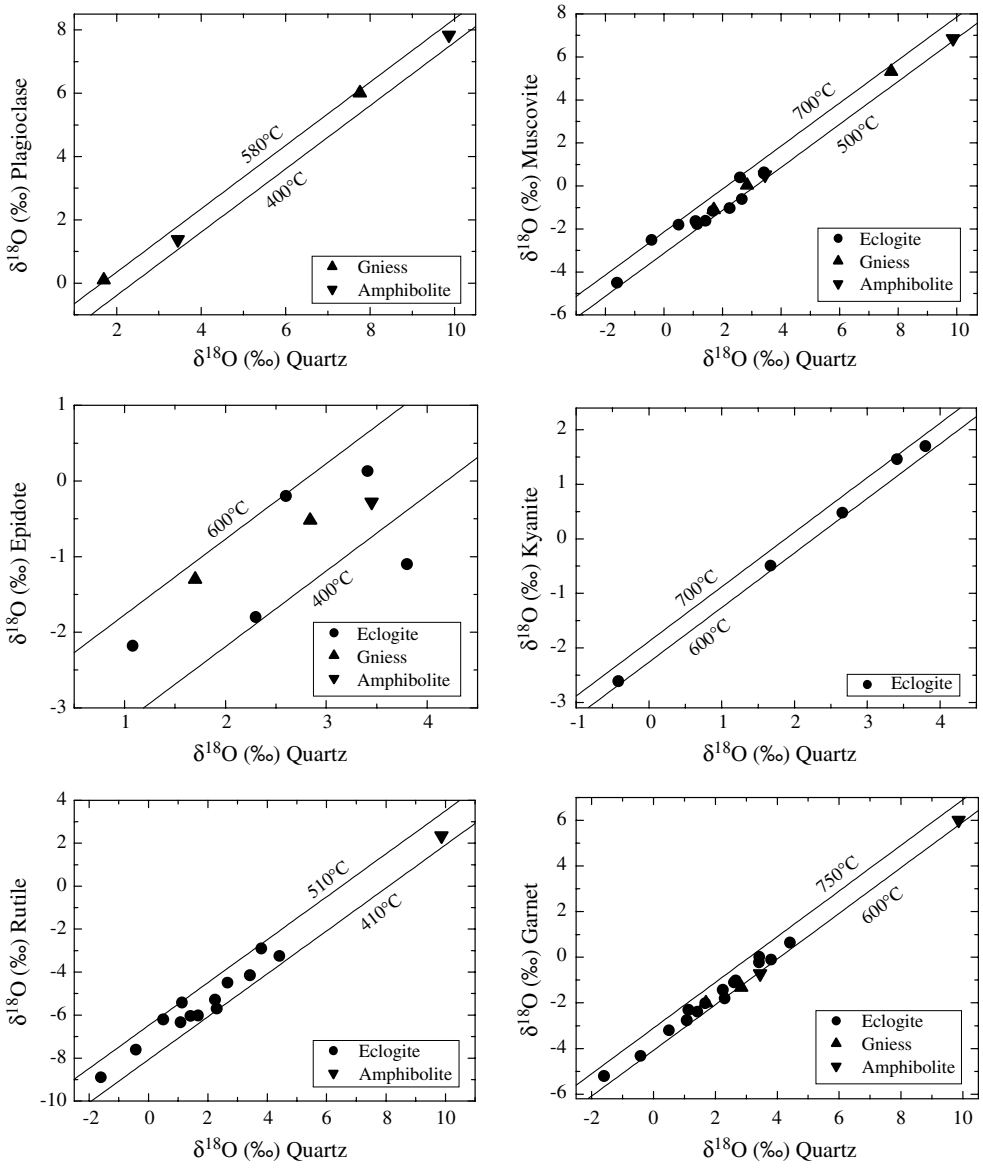

Fig. 14 Plots of the O isotope composition of quartz versus the O isotope compositions of coexisting minerals in eclogite, garnet amphibolite and gneiss from the Huangzhen-Zhujiachong area in South Dabie (data from this study and Zheng et al. 1999). Slope = 1 equilibrium fractionation lines at different temperatures are drawn by applying the theoretical calibrations of Zheng (1991, 1993a, 1993b)

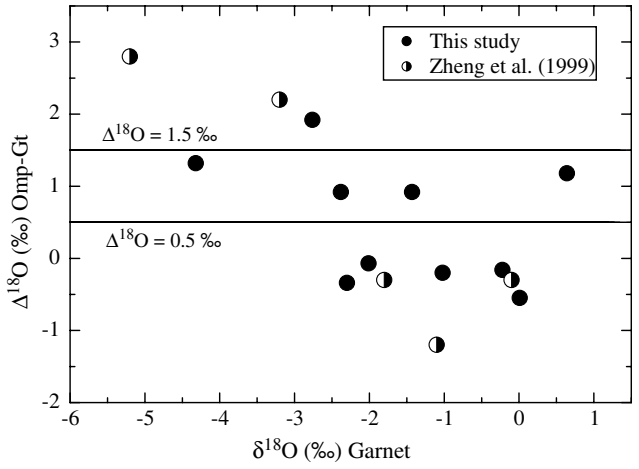

Fig. 15 Oxygen isotope fractionations between omphacite and garnet versus the $\delta^{18}O$ values of garnet in eclogites from the Huangzhen-Zhujiachong area in South Dabie (data from this study and Zheng et al. 1999). The reference lines of $\Delta^{18}O = 0.5‰$ and 1.5‰ place limits of equilibrium fractionation between omphacite and garnet, and the samples beyond the two lines are out of isotopic equilibrium

395∼421 Ma at the low-T heating steps may imply a significant replacement of Na to K during paragonite crystallization. The normal isochron fitting was conducted by using the ISOPLOT program, yielding an age and an initial $^{40}Ar/^{36}Ar$ ratio of 245.5 ± 9.8 Ma and 293.1 ± 4.1, respectively (Fig. 12b). The isochron age of this paragonite is in good agreement with its plateau age, and its initial $^{40}Ar/^{36}Ar$ ratio is consistent with the $^{40}Ar/^{36}Ar$ ratio of 295.5 for the modern atmosphere Ar. Therefore, the Ar–Ar ages of 241.3–245.5 Ma date paragonite crystallization during metamorphism.

Whole-rock Nd and Sr isotopes

In order to constrain the nature of eclogite protolith, Sm–Nd and Rb–Sr isotope compositions were analysed for six whole-rock samples from the low-T eclogite (Table 5). The Sm–Nd results show small variations in both $^{147}Sm/^{144}Nd$ and $^{143}Nd/^{144}Nd$ ratios of 0.1200–0.1359 and 0.512004–0.512203, respectively. In terms of zircon U–Pb ages of $t_2 = 230$ Ma and $t_1 = 1{,}800$ Ma for metamorphic event and magma emplacement (Figs. 9 and 10), respectively, initial $^{143}Nd/^{144}Nd$ ratios were calculated to yield $\varepsilon_{Nd}(t_2)$ values of -10.1 to -6.7 but $\varepsilon_{Nd}(t_1)$ values of 4.7–6.0 (Table 5). Initial $^{87}Sr/^{86}Sr$ ratios so calculated are $I_{Sr}(t_2)$ values of 0.70535–0.70637 and $I_{Sr}(t_1)$ values of 0.70404–0.70484. Nd model ages were calculated by using a single-stage model relative to the depleted mantle (DePaolo 1988), which gave a T_{DM} range from 1.8 to 1.9 Ga (Table 5). The Nd model ages are close to the zircon U–Pb discordia age of $1{,}817 \pm 102$ Ma for the upper intercept (Fig. 10a), and the $\varepsilon_{Nd}(t_1)$ values of 4.7–6.0 are consistent with the Nd isotope composition of the depleted mantle (Fig. 13). These results indicate that protolith of the low-T eclogite has the geochemical nature of paleoceanic basalt that was derived from the depleted mantle by magmatism at about 1.8–1.9 Ga. The occurrence of ca. 1.8 Ga zircon in the eclogite indicates either recycling of crustal material into the mantle source or formation of zircon in the metasomatised mantle during the late Paleoproterozoic. The slightly higher $I_{Sr}(t_1)$ values of 0.70404–0.70484 at 1,800 Ma relative to the primary mantle (Fig. 13) may be caused by seawater-hydrothermal alteration during the basalt eruption.

Mineral O and H isotopes

O and H analyses were previously carried out for single minerals from eclogite and gneiss as well as associated quartz veins within the low-T eclogite (Zheng et al. 1999; Li et al. 2001; Xiao et al. 2002). In addition to the previous database, a number of samples were collected from the Huangzhen-Zhujiachong area for O and H isotope analyses, and the results are listed in Table 7.

Ten eclogite samples show $\delta^{18}O$ values of -4.3 to 0.6‰ for garnet, -3.0 to 1.8‰ for omphacite, and -0.4 to 4.4‰ for quartz (Table 7). Two garnet amphibolite samples show $\delta^{18}O$ values of -0.7 to 6.0‰ for garnet, -0.8 to 6.4‰ for amphibole, and 3.5–9.9‰ for quartz. For gneiss, two samples show $\delta^{18}O$ values of 0.1–5.3‰ for muscovite and 2.8–7.8‰ for quartz. The eclogites are estimated to have $\delta^{18}O$ values of -4 to 3‰ when normalized to whole-rock composition, which are consistent with the previous results of Zheng et al. (1999) and Xiao et al. (2002). It appears that the low-T eclogites are variably depleted in ^{18}O relative to the normal mantle composition, with significant $\delta^{18}O$ heterogeneity. According to the fractionation factors of Zheng et al. (1991, 1993a, b), O isotope temperatures are calculated from fractionations between quartz and the other minerals (Table 7). The results show that most of the quartz-mineral pairs are in isotopic equilibrium with respect to eclogite-facies metamorphism and subsequent cooling (Fig. 14). Quartz–garnet and quartz–kyanite pairs appear to be in isotopic equilibrium, yielding relatively narrowed temperature ranges of 630–695°C and 620–690°C, respectively. By contrast, quartz–omphacite pairs yield a large temperature range of 690–415°C (Table 7), most of them being with disequilibrium fractionations between coexisting omphacite and garnet (Fig. 15). Mineral pairs that contain zoisite/epidote also yield a large temperature range of 590–425°C, which is lower than the temperatures of the eclogite-facies metamorphism but compatible with the closure temperatures of O diffusion in the minerals during retrograde metamorphism (Zheng and Fu 1998).

The H isotope compositions of hydroxyl-bearing minerals in the eclogite, garnet amphibolite and gneiss show a δD range of -89 to -77‰ for paragonite/muscovite, -75 to -54‰ for zoisite/epidote, and -85 to -83‰ for amphibole (Table 7). The sequence of D-enrichment in the coexisting minerals is not compatible with that predicted from experimental studies under

hydrothermal conditions (Suzuoki and Epstein 1976; Graham et al. 1980, 1984) for equilibrium fractionation at temperatures above 500°C (muscovite > amphibole > biotite > epidote > zoisite), indicating H isotope disequilibrium among the hydroxyl-bearing minerals. Experimental studies of H isotope exchange kinetics show that the rate of H diffusion in hydroxyl-bearing minerals is mica < amphibole < epidote (Graham 1981). The rate of H isotope exchange between hydroxyl-bearing mineral and water is much faster than O isotope exchange in the same system (Graham 1981; Zheng and Fu 1998). Therefore, the H isotope disequilibrium among the hydroxyl-bearing minerals from the Dabie metamorphic rocks is due to differential exchange with the retrograde fluid during exhumation. The decompression exsolution of hydroxyl from nominally anhydrous minerals such as omphacite, garnet and rutile has been documented to be an important source of retrograde fluid in exhumed eclogites (Zheng et al. 1999, 2003a; Li et al. 2001).

The O isotope temperatures of 620–695°C calculated from the fractionations between quartz and refractory minerals from the eclogite samples are consistent with the petrological estimates of peak metamorphism at about 670°C in this study and the other studies at 650–700°C (Zhai et al. 1995; Castelli et al. 1998). This suggests preservation of O isotope equilibrium at the eclogite-facies temperatures and thus preservation of pre-metamorphic $\delta^{18}O$ values for precursors of both eclogite and gneiss before plate subduction.

The O and H isotope disequilibria between some of the minerals have been obviously caused by retrograde reactions as described in the previous sections. The retrograde reactions have not achieved isotopic reequilibration, but differential isotopic exchange has taken place between the minerals and retrograde fluid (Zheng et al. 1998, 1999). According to the feature of O isotope compositions in both quartz vein and host eclogite, it was inferred that the $\delta^{18}O$ value of retrograde fluid is variable, but internally buffered, depending on the nature of host rocks (Li et al. 2001). This results in the decrease in O isotope temperature for such minerals as epidote, rutile, amphibole and mica that are readily susceptible to retrograde isotope exchange. Garnet and kyanite are very resistant to O isotopic exchange during retrograde alteration to the eclogite minerals and thus have probably preserved their primary $\delta^{18}O$ values that were acquired during the UHP metamorphism. The O isotope disequilibrium between omphacite and garnet is principally caused by the symplectitic replacement of omphacite and differential isotope exchange with the retrograde fluid.

Discussion

Breakdown of lawsonite and origin of retrograde fluid

The lack of chemical zonation in the omphacite coexisting with well-zoned garnet may be due to partial chemical reequilibration of omphacite during metamorphic processes. Theoretical and experimental studies documented that garnet is chemically sluggish in compositional reequilibration (Lasaga 1983). The textural evidence in this study as well as the previous studies (e.g., Zhai et al. 1995; Castelli et al. 1998) also indicate that garnet is much more resistant to retrogression so that its chemical zonation is still well persevered. It has been observed in this study that garnet in the veins has no compositional zonation, but has the similar chemical composition to the garnet rim in the host eclogite. This implies that the garnets formed probably also around peak metamorphic conditions before or during the lawsonite breakdown into the pseudomorphic assemblage.

The formation of lawsonite eclogite during the subduction period indicates that the eclogite protolith is probably enriched in CaO and Al_2O_3. Compositional growth zoning in garnet records a progressive evolution from lawsonite blueschist-facies progressing to lawsonite eclogite-facies. The textures of post-peak metamorphic reaction include amphibole-plagioclase intergrowths after omphacite, and the replacement of kyanite by plagioclase-bearing symplectites. The potential preservation of lawsonite without decomposition during plate subduction in the transition from blueschist-facies to eclogite-facies was probably favored by a rapid subduction of the Yangtze continental plate in the Triassic (Zheng et al. 1999, 2003a). Clinozoisite could form from both prograde and retrograde metamorphism and was stable over a large *P–T* range in metamorphic rocks of normal mafic composition. The pervasive existence of clinozoisite in the low-T eclogites implies a water-rich precursor.

The *P–T* path of the investigated eclogites shows a typical history related to the processes of both subduction and exhumation (Fig. 8a). When the subducted slab started to dehydrate, lawsonite probably formed at the onset of prograde HP metamorphism under the water-rich conditions of about 250°C and 0.2–0.5 GPa. The growth of lawsonite could be at the expense of chlorite, glaucophane, zoisite and plagioclase as well as H_2O and Ca-bearing minerals (e.g. Okay 1980; Will et al. 1998; Ballever 2003). In the case of the subduction of a very old oceanic crust along an extremely low geothermal gradient (2– 3°C/km), the subducting oceanic crust would suffer progressive LT/HP metamorphism from blueschist- to lawsonite eclogite-facies (Okamoto and Maruyama 1999). The zircon U–Pb dating in eclogite sample 97H05 has detected the very old cores of 1,729–1,849 Ma (Fig. 9), indicating the survival of protolith signature during the Triassic UHP metamorphic event. Reconstructed mineral assemblage of blueschist was transformed into that of lawsonite eclogite under the conditions of 1.5–2.0 GPa and 450–550°C (Liou et al. 1998; Okamoto and Maruyama 1999). The most important reaction for this transformation would be: epidote + glaucophane = garnet + omphacite + paragonite + quartz + H_2O. Lawsonite-bearing eclogite is stable in cold subduction zones of low-T/

UHP, but may suffer transformation into zoisite-bearing eclogite with decreasing pressure when the UHP slab started to exhume from the mantle depth. It appears that the transition from blueschist-facies to eclogite-facies is temperature dependent (Fig. 8a), differing from the pressure-dependent transition of amphibolite to eclogite or granulite to eclogite at high temperatures. Therefore, the rocks experienced the peak *P–T* conditions at 3.3 GPa and 670°C, and followed near-isothermal decompression to 1.8 GPa and 680°C.

During the initial exhumation of UHP slab, lawsonite became unstable with decompression across its stable reaction line and dehydrated to form the kyanite + zoisite + coesite assemblage at first (Fig. 8a). The *P–T* path of the investigated quartz–kyanite veins also shows an exhumation-related history (Fig. 8b). Although the timing for formation of the kyanite–quartz vein may be close to 226 ± 6 Ma (Fig. 10b), the mineral assemblage and the garnet composition within the vein highlight its formation at eclogite-facies subsequent to the peak UHP metamorphism. There is little sign of recrystallization of the large quartz crystal into aggregates of finer grains with prefect orientation, even though coarse-grained quartz occasionally exhibits undulose extinction and kink-bands. Such a textural relationship indicates that the kyanite–quartz veins did not undergo intensive deformation or plastic flow. No foliation, strong fracturing and undulose extinction was observed from the quartz, so that the kyanite–quartz veins are assumed to develop after the peak UHP metamorphic stage when the compressional subduction was transformed to the decompression exhumation with potential generation of extensional fractures. This is also confirmed by calculations of phase equilibrium curves on the reaction of lawsonite breakdown to the Ky–Zo–Qtz assemblage (Fig. 8b). The formation of kyanite–quartz vein observed in the low-T eclogite would result from the transition of lawsonite eclogite to epidote eclogite during the initial exhumation. At this transiting process, water was released to carry dissolved SiO_2 from the host eclogite and deposit it in the fracture as veins. The veins developed more easily along the lawsonite-rich area, resulting in an easier observation of the lawsonite pseudomorphs or Ky–Zo–Qtz assemblage in veins than that in the host eclogite.

The breakdown of lawsonite would occur at the onset of exhumation when the UHP slab started to decompress during the initial exhumation, and thus took place in the transition zone (Fig. 8) of lawsonite eclogite to epidote eclogite (Liou et al. 1998; Okamoto and Maruyama 1999). The breakdown *P–T* conditions of lawsonite are well consistent with the experimental results (Pawley 1994; Poli and Schmidt 1997; Schmidt and Poli 1998; Okamoto and Maruyama 1999; Forneris and Holloway 2003). The peak *P–T* conditions are significantly higher than the previous estimates for the low-T eclogites. In particular, the occurrence of coesite pseudomorphs (Fig. 3) upgrades the HP unit in the Huangzhen-Zhujiachong area to an UHP unit. As the decompression continued, the rock entered the amphibole eclogite field with almost no increase in temperature.

In the processes of transition from lawsonite eclogite to epidote eclogite and then amphibole eclogite, fluid was internally buffered chemically. It is likely that the breakdown of lawsonite provides water for the transformation of omphacite into amphibole in addition to the hydroxyl exsolution. Greenschist-facies overprinting is not obvious in both vein and eclogite. The retrograde fluid was an important exchange medium to cause both disequilibrium of O isotope fractionations between omphacite and garnet in the eclogite and disequilibrium of H isotope fractionations between epidote and mica in the eclogite, gneiss and amphibolite (Table 7 and Fig. 15). The fluid for retrograde reactions was internally buffered in the stable isotope compositions. In other words, the retrograde metamorphism would take place in relatively closed systems for isotopic compositions, and the O and H isotope compositions of retrograde fluid would be similar to those of the host rocks.

The low $\delta^{18}O$ values of -4 to $3‰$ for the eclogite whole-rock and the low δD values of -89 to $-77‰$ for paragonite from the eclogite (Table 7) indicate the incorporation of surface water into the eclogite protolith by high-T hydrothermal alteration. The fluid inclusions in the minerals of low-T eclogite also have low salinity (Fu et al. 2003b). Appropriate amounts of aqueous fluid are thus implicated in the altered protolith (paleoceanic basalt) during the prograde UHP metamorphism. With respect to its exact origin from seawater or meteoric water for the pre-metamorphic fluid, however, we have to take into account the complicated history that the Dabie-Sulu eclogites had experienced. It is known that most of UHP eclogites in the Dabie-Sulu orogenic belt have their protoliths from continental basalt and gabbro that were emplaced in the middle Neoproterozoic (700–800 Ma) along the northern margin of the Yangtze plate and that underwent a large-scale meteoric-hydrothermal alteration together with coeval granitoids in the same period of rift magmatism (Jahn 1998; Zheng et al. 1998, 1999, 2003a, b, 2004; Rumble and Yui 1998; Rumble et al. 2002). As a result, extremely low $\delta^{18}O$ values of -10 to $-5‰$ and δD values of -127 to $-100‰$ have been observed for the eclogite protoliths of the Neoproterozoic age. In contrast, the low-T eclogite in South Dabie has its protolith from the paleoceanic basalt that erupted in the late Paleoproterozoic (1.8–1.9 Ga) and thus served as the country rock during the Neoproterozoic emplacement of bimodal magmas along the rifting tectonic zones. In addition to the previous seawater-hydrothermal alteration during the paleoceanic basalt eruption, the protolith of the low-T eclogite may also have suffered the high-T meteoric-hydrothermal alteration triggered by the bimodal magmatism during the middle Neoproterozoic. In this context, sufficient fluids were available within the low-T eclogite protolith to form lawsonite during the prograde UHP metamorphism by the Triassic continental subduction.

Fluid activity during exhumation

The hydrous Ca-bearing minerals such as zoisite and lawsonite were proven by the experiments to be stable at very high pressures, up to 5.0 GPa for zoisite (Poli and Schmidt 1998; Grevel et al. 2001) and greater than 12.0 GPa for lawsonite (Poli and Schmidt 1997; Okamoto and Maruyama 1999), and are therefore potential carriers of water into the Earth's mantle during plate subduction. Lawsonite is a special rock-forming mineral that can store more than 10 wt% water. It may occur not only in mafic and intermediate meta-igneous rocks, but also in carbonate-bearing metasediments. The equilibrium conditions for the dehydration of lawsonite to zoisite, kyanite and quartz/coesite are at pressures and temperatures up to 5.0 GPa and 850°C (Schmidt and Poli 1998; Grevel et al. 2001; Forneris and Holloway 2003). In common mafic rocks, lawsonite is a promising hydrous phase present at pressures of 5.0 GPa, and stable to temperatures at ca. 700°C.

The H_2O components from the fluid phase could be carried down into subduction zones up to UHP metamorphism, and released by the breakdown of lawsonite to form the Ky–Zo–Qtz assemblage as demonstrated in this study. Castelli et al. (1998) also reported the lawsonite pseudomorph, which was replaced by kyanite, zoisite and quartz in the metamorphic veins within the low-T eclogite at Zhujiachong in South Dabie, which belongs to one of the presently investigated localities. They considered that the lawsonite breakdown occurred during the prograde metamorphism of low-T eclogite-facies in a transition from lawsonite to zoisite stability field. Our conclusion of the lawsonite breakdown at the onset of initial exhumation is based on the relationship between the calculated P–T path and metamorphic reactions as well as the absence of foliation texture, and undulose extinction of the quartzes in the veins. These observations at least indicate that the low-T eclogites in the Huangzhen-Zhujiachong area are rich in fluids during the prograde UHP metamorphism. The fluid for forming lawsonite could result from two sources, i.e., dehydration of subducted slab from surrounding sediments and the interior of the altered basalts.

It is usually assumed that the dehydration of oceanic crusts begins when subduction starts, but leaves the water-undersaturated portion moving towards H_2O-saturation as a result of prograde P–T evolution and increasing H_2O-availability (Poli and Schmidt 1997). Thus, the bulk dehydration does not mean a result toward H_2O-poor rocks, but more relevant to H_2O saturation, because fluid-release is impossible if H_2O-satuation is not attained (Poli and Schmidt 1997). It is thus important to understand that the development of zoisite on lawsonite or zoisite pseudomorph after lawsonite could occur during exhumation processes. It is possible that the fluid released from lawsonite could enter the surrounding rocks to result in the formation of veins internally when UHP rocks experienced a near-isothermal decompression from the UHP eclogite-facies metamorphism to the HP eclogite-facies recrystallization and amphibolite-facies retrogression. Fluid generation and vein formation were also suggested by Cartwright and Buick (2000) to occur during decompression of high-pressure terranes in the Schistes Lustres of Alpine Corsica, France. On the other hand, replacement of lawsonite by zoisite could occur as a result of the formation of retrograde garnet rims with enriched MgO and FeO, which is also consistent with the zoned patterns of our garnet (Fig. 6). As a consequence, developments of zoisite after lawsonite would not cause a fluid release (Poli and Schmidt 1997). In either case, lawsonite is sensitive to the increase in temperature corresponding to the decrease in pressure. This is probably the reason why no lawsonite has been preserved in retrograded UHP or HP eclogites from the Dabie-Sulu orogenic belt.

The local distribution of kyanite–quartz veins within the low-T eclogite indicates that the whole-rock chemistry of eclogite controlled their occurrence and that the vein-forming fluid was at least partly locally derived. This is supported by the observed Nd and Sr isotope features with heterogeneous $\delta^{18}O$ values for the host eclogites in this study. The previous O and H isotope studies of Zheng et al. (1998, 1999, 2003a) for the eclogites from the Dabie terrane including the Huangzhen-Zhujiachong area have also indicated that the fluid from retrograde reactions was internally buffered in the stable isotope compositions. It was thus proposed that the retrograde fluid was derived from exsolution of structural hydroxyl dissolved in nominally anhydrous minerals (Zheng et al. 1999, 2003a; Li et al. 2001). This hypothesis has gained more and more support from the recent measurement of hydroxyl content in such nominally anhydrous minerals as omphacite, garnet, rutile and jadeite (Zhang et al. 2001, 2004; Katayama and Nakashima 2003; Sheng et al. 2004; Su et al. 2004). The present study demonstrates that the breakdown of lawsonite at the onset of exhumation subsequent to peak UHP metamorphism may also have offered considerable amounts of aqueous fluid for retrograde metamorphism and veining.

The subduction zone could be the only channel to carry the water into the depth of the Earth (Ernst 2001), but aqueous fluid may sufficiently be released during the subduction of young and hot oceanic crust to generate arc volcanism. By means of experimental studies Forneris and Holloway (2003) demonstrated that the basaltic layer of a slab would be completely dehydrated between 90 and 110 km depth in a subduction zone at a temperature of about 645°C. Spandler et al. (2003) suggested that approximately 3–4 wt% water of mafic rocks was liberated during the transition from lawsonite blueschist (4–5 wt% water) to eclogite (< 1 wt% water). The previous experimental results (e.g., Poli and Schmidt 1997; Schmidt and Poli 1998; Forneris and Holloway 2003) also demonstrated that lawsonite breakdown is mainly temperature-dependent, but the modal amount of any hydroxyl-bearing mineral decreases greatly with

temperature and pressure increase in a subducting slab. After the peak UHP metamorphism of oceanic crust, if any hydroxyl-bearing mineral was still present, the modal amount would be very limited because of the sufficient dehydration. In the case of the subduction of young and hot oceanic crust, therefore, it is possible that quartz–kyanite veins would usually form during prograde dehydration and that lawsonite breakdown would normally occur during the prograde metamorphism of eclogite in a transition from lawsonite to zoisite stability field.

During the deep subduction of old and cold continental crust, on the other hand, the volatile and water were encluded as structural hydroxyl and nano-scale inclusions in hydrous and nominally anhydrous minerals (Zheng et al. 2003a); because of the rapid nature of continental subduction, they were not able to be sufficiently released to generate syn-subduction magmatism like arc volcanics that is typical of oceanic crust subduction. On the basis of the *P–T* conditions estimated in this study, nevertheless, lawsonite could bring the water into the mantle depth >100 km during subduction of the continental crust in the Dabie-Sulu orogenic belt, and, therefore, affect the rheology of the upper mantle. During the exhumation, however, significant amounts of aqueous fluid would be librated from both lawsonite decomposition and hydroxyl exsolution due to pressure decrease, resulting in pervasive amphibolite-facies retrogression, quartz veining and syn-exhumation magmatism (Zheng et al. 2003a). The syn-exhumation K-rich granites with emplacement ages of Late Triassic have been reported to occur in the Qinling-Dabie-Sulu orogenic belt (Zhang et al. 2001; Sun et al. 2002; Chen et al. 2003). In addition to heat supply by the mantle upwelling subsequent to plate breakoff (Davis and von Blanckenburg 1995; Atherton and Ghani 2002), the decompression exsolution of K and OH from UHP minerals is a critical mechanism to trigger the partial melting of overlying rocks within exhumed slab by decreasing the melting temperature.

Implications for radiometric dating during subduction and exhumation

Triassic ages for the UHP metamorphism in the Dabie-Sulu orogenic belt were obtained by zircon U–Pb, mineral Sm–Nd, Rb–Sr and Ar–Ar dating for eclogites and gneisses, ranging from 245 to 210 Ma (e.g., Li et al. 1993, 1994, 2000; Okay et al. 1993; Ames et al. 1996 ;Chavagnac and Jahn 1996; Rowley et al. 1997; Hacker et al. 1998; Webb et al. 1999; Ayers et al. 2002). However, the exact timing of UHP metamorphism is still controversial. One school interprets the UHP event to occur at Late Triassic according to the zircon U–Pb ages of 210–225 Ma (Ames et al. 1996; Rowley et al. 1997) and mineral Sm–Nd isochron ages of 210–226 Ma (Li et al. 1993, 1994, 2000; Chavagnac and Jahn 1996). The other advocates the peak UHP metamorphism to take place at Early-Middle Triassic on the basis of a few Sm–Nd mineral isochron ages of ~245 Ma for eclogites (Li et al. 1993, 2000; Okay et al. 1993), a SHRIMP U–Pb age population of ~240 Ma overgrowths on single zircon grains in granitic gneisses (Hacker et al. 1998), and zircon and monazite CAMECA U-Th-Pb ages of 230–238 Ma (Ayers et al. 2002). It appears that a resolution to this controversy necessitates comprehensive investigations concerning not only a combined study of zircon growth history and U–Pb radiometric dating but also a correct understanding of Pb and Nd diffusivity in radiometrically dated minerals during prograde and retrograde metamorphic processes (Zheng et al. 2002, 2003c). The present study of zircon U–Pb, mineral Sm–Nd and Rb–Sr, and paragonite Ar–Ar dating can shed light on this aspect.

Zircon found in eclogite-facies rocks can be inherited from protolith or form by prograde or retrograde metamorphism during subduction or exhumation. Metamorphic zircon can form by solid-state or anatectic recrystallization, and growth or overgrowth due to metamorphic reactions, dissolution/precipitation, or even aqueous fluid circulation at variable pressure and temperature conditions. Fluid availability plays a critical role in dictating zircon growth or overgrowth during high-grade metamorphism (e.g., Roberts and Finger 1997; Liati et al. 1999; Rubatto et al. 1999; Rubatto and Hermann 2003). Under conditions of fluid absence, in particular, either recrystallization or growth of zircons can efficiently be prohibited during peak UHP eclogite-facies and HP granulite-facies metamorphism (Zheng et al. 2004). Upon to the progressive subduction into the regime prior to the peak UHP conditions, paragonite is expected to decompose when across its stable reaction line (Fig. 8a), resulting in the formation of Ky-Omp assemblage with H_2O release. During this process an aqueous fluid was available for mineral reaction and zircon growth over a prograde *P–T* range within low-T/high-P eclogite-facies (point B in Fig. 8a). Thus the first group SHRIMP age of 242 ± 3 Ma in Fig. 10b may date zircon growth at Early Triassic in the course of continental subduction prior to the onset of peak UHP conditions.

On the other hand, lawsonite would breakdown to form the Ky–Zo–Coe assemblage with possible H_2O release when the UHP slab started to decompress at the onset of exhumation (Fig. 8a). This process can offer an aqueous fluid for zircon growth/overgrowth over a retrograde *P–T* range under conditions of HP eclogite-facies and for the formation of quartz veins. As a result, the second group SHRIMP age of 222 ± 4 Ma in Fig. 10b may date zircon overgrowth at Late Triassic during the exhumation in response to decompression dehydration in the course of high-P eclogite-facies to upper amphibolite-facies retrogression (point D in Fig. 8a). This is consistent with apparent $^{206}Pb/^{238}U$ ages of 214–221 Ma for rutile of quartz veins within the low-T eclogite at Huangzhen and Lidu in South Dabie (Franz et al. 2001). In addition, the retrograde fluid within the exhumed UHP slab became more available due to the decompression exsolution of hydroxyl dis-

solved in nominally anhydrous minerals, resulting in pervasive amphibolite-facies retrogression and local veining (Zheng et al. 1999, 2003a; Li et al. 2001). The quartz veins within the eclogites in the Dabie-Sulu orogenic belt were thus formed by cyclic circulation of aqueous fluids that were locally derived from dehydration reactions at the transition of UHP to HP eclogite-facies during exhumation.

The mineral Sm–Nd and Rb–Sr isochron dates for the low-T eclogite yield the concordant ages of middle Triassic at 236.1 ± 4.2 Ma and 230 ± 7 Ma, respectively (Fig. 11). These ages just lie between the two group ages of zircon U–Pb dating (Fig. 10b), and are similar to, but slightly older than, previous dates by the Sm–Nd method on the MT/UHP eclogites in Central Dabie, for example, of 226 ± 3 Ma for the Shuanghe eclogite (Li et al. 2000) and 225 ± 7 Ma for the Bixiling eclogite (Chavagnac and Jahn 1996). The O isotope equilibria were achieved and preserved between the isochron minerals (Table 7 and Fig. 14), providing a test of Nd and Sr isotopic equilibria in the dated minerals (Zheng et al. 2002, 2003c). Although the closure temperatures of O diffusion may not simply correspond to those of Sr or Nd diffusion in eclogite minerals formed at different *P*–*T* conditions, Sr and Nd isotopic equilibria are evident from the consistent ages of middle Triassic (Fig. 11). Therefore, both Sm–Nd and Rb–Sr systems attained and preserved their radiometric isotope equilibration between the eclogite minerals during the Triassic UHP metamorphism.

Since Nd and Sr isotope transports in high-T systems are principally dictated by element diffusion between minerals, the present study provides a possible constraint on the timing of peak UHP metamorphism at sometime prior to about 236.1 ± 4.2 Ma. In this regard, the age of peak UHP metamorphism may be different in different occurrences or localities of eclogite if they are responsible for different slices of deep-subducted slab. The LT/UHP "cold" eclogite unit in this study is located between the LT/HP blueschist-facies unit and the MT/UHP "hot" eclogite-facies unit (Fig. 1). Its protolith is the hydrothermally altered paleoceanic basalt of Paleoproterozoic age, whereas the protolith of MT/UHP eclogites is the hydrothermally altered continental basalt and gabbro of Neoproterozoic age. In the processes of progressive subduction, the eclogite protoliths of different occurrences would be located in different layers within the subducted plate and thus suffered different degrees of mineralogical and geochemical transformation depending on protolith nature and fluid availability. The older Sm–Nd isochron age of 236.1 ± 4.2 Ma for the LT/UHP eclogite than the Sm–Nd isochron ages of 226 ± 3 to 225 ± 7 Ma for the MT/UHP eclogites may imply that the former protolith would run out of the peak UHP conditions about 10 Ma earlier than the latter ones if the mineral Sm–Nd isochron would have dated the minimum ages of peak UHP event.

The Ar–Ar dating on the paragonite shows the good agreement between the plateau and isochron ages (Fig. 12), with the initial $^{40}Ar/^{36}Ar$ ratio close to the $^{40}Ar/^{36}Ar$ ratio of the atmosphere Ar. These indicate that the paragonite did not trap excess Ar during its crystallization. No significant resetting of the K–Ar isotopic system took place during the post-peak metamorphism in the course of eclogite exhumation. Therefore, the plateau and isochron ages of 241.3 ± 3.1 and 245.5 ± 9.8 Ma date the paragonite crystallization during the prograde eclogite-facies metamorphism (point B in Fig. 8a). This seems to imply either a high closure temperature for Ar diffusion in paragonite or a rapid quench during the initial exhumation. However, it is unclear why the exhumation-related metamorphism did not reset the K–Ar system of paragonite to the Late Triassic age. The preservation of the Early Triassic age, nevertheless, indicates very limited mobility of Ar in paragonite during UHP metamorphism. This suggests that paragonite, a K-poor mica, may enclose its radiometric Ar in lattice defects as micro-inclusions during its crystallization and thus is capable of preserving its radiometric Ar without resetting by the subsequent UHP metamorphism.

All the available radiometric dates on the UHP eclogites from the Dabie-Sulu orogenic belt indicate a possible timescale of bulk continental subduction and exhumation from ca. 245∼240 to 225∼220 Ma in the HP-UHP-HP regimes. In the processes of continental subduction and exhumation, the closure of radiometric systems in the UHP minerals is expected to occur considerably some time after the attainment of the maximum subduction depth. As a consequence, the real age of UHP metamorphic event is considerably older than the mineral Sm–Nd isochron ages because the UHP metamorphic conditions are defined by the maximum pressure rather than the maximum temperature. Even if the peak metamorphic temperatures attained are close to the closure temperatures for the mineral Sm–Nd system, the protracted process of near-isothermal exhumation in the eclogites would reset the radiometric clock to result in the cooling age. In this context, the mineral Sm–Nd isochron ages may record the time at which the retrograde isotope exchange ceased due to varying availabilities of fluid within the UHP rocks during the initial exhumation. Therefore, the possible period of UHP metamorphism is bracketed at about 240–230 Ma. In this regard, zircon growth is expected to occur principally in two periods, respectively, when the fluid became available. One is about 245–240 Ma that took place prior to the onset of peak UHP metamorphism, and the other is about 230–220 Ma that run out of the peak UHP conditions. This expectation can be tested if zircon domains that contain coesite are in-situ dated by the SIMS technique.

The above estimates of peak UHP metamorphic event provides a possible constraint on the maximum duration of bulk HP-UHP-HP metamorphic processes in about 15–25 Ma. This duration is in general agreement with the previous estimate from the O isotope study of eclogite minerals that the UHP metamorphism in the Dabie-Sulu orogenic belt occurred in a short

duration of 5–10 Ma (Zheng et al. 1998), but that bulk recycling of continental subduction, UHP metamorphism at mantle depths and exhumation lasted on the order of 10–20 Ma (Zheng et al. 2003a). A possible duration of about 12–26 Ma was estimated by Zheng et al. (2003d) for effective diffusion transport at 850–600°C towards Sr isotope reequilibration but failure of O isotope equilibration between minerals of garnet peridotite in the Sulu terrane.

Conclusions

Coesite pseudomorph was found in the low-T eclogite between the southern low-T/high-P blueschist-facies unit and the northern medium-T/UHP eclogite-facies unit, upgrading the low-T/high-P eclogite-facies unit into a low-T/UHP unit. Petrographic and mineralogical studies of the eclogite and associate kyanite–quartz veins as well as thermodynamic calculations demonstrate that the low-T eclogite experienced UHP metamorphism at the peak P–T conditions of 670°C and 3.3 GPa. The pervasive occurrence of Ky–Zo–Qtz aggregation in the eclogite as pseudomorph after lawsonite indicates a possible breakdown of lawsonite at the onset of exhumation process when lawsonite eclogite transformed into epidote eclogite.

Studies of mineral O and H isotopes indicate that eclogite protolith was depleted in ^{18}O before continental subduction and thus experienced hydrothermal alteration by surface waters. The low and heterogeneous $\delta^{18}O$ values for the low-T eclogite indicate that the fluid for retrograde reactions was internally buffered in stable isotope composition. The formation of kyanite–quartz veins are petrologically and thermodynamically consistent with the early exhumation of UHP metamorphic slab when the lawsonite brokedown into the Ky–Zo–Qtz aggregation. In addition to the hydroxyl exsolution from nominally anhydrous minerals (Zheng et al. 1999, 2003a; Li et al. 2001), the breakdown of lawsonite would provide significant amounts of aqueous fluid for retrograde metamorphism and vein formation.

Zircon U–Pb, mineral Sm–Nd and Rb–Sr, and paragonite Ar–Ar dating demonstrates that the low-T eclogite also underwent the Triassic UHP metamorphism like those in Central Dabie. Eclogite Nd and Sr isotope analyses together with the zircon U–Pb age indicate that the eclogite protolith would be the paleoceanic basalt derived from the depleted mantle by magmatism at about 1.8–1.9 Ga, but experienced the two episodes of hydrothermal alteration, respectively, by seawater during the magma eruption in the late Paleoproterozoic and by meteoric water during rifting magmatism in the middle Neoproterozoic along the northern margin of the Yangtze plate. As a result, sufficient amounts of aqueous fluid were available from the eclogite protolith itself for lawsonite formation during the prograde UHP metamorphism by the Triassic continental subduction.

Isothermal decompression subsequent to the peak pressure triggered the second episode of fluid release by lawsonite breakdown. While the paragonite Ar–Ar age of 241.3 ± 3.1 Ma is interpreted to represent the timing of paragonite crystallization during progressive HP metamorphism, the zircon U–Pb ages of 242 ± 3 Ma and 222 ± 4 Ma dated zircon growth and overgrowth in the two episodes of dehydration, respectively, in response to decomposition of water-bearing minerals such as glaucophane, epidote and paragonite during deep subduction and the lawsonite breakdown during initial exhumation. The timing of peak UHP metamorphism is constrained at sometime prior to about 236.1 ± 4.2 Ma for the low-T eclogite, the bulk period of UHP metamorphism is estimated to occur in a range of about 240–230 Ma for different occurrences of eclogite in the Dabie-Sulu organic belt. Thus the termination age of peak UHP metamorphism is probably different in different slices of deep-subducted slab. The timescale of bulk continental subduction and exhumation in the HP-UHP-HP regimes may range from ca. 245∼240 Ma to 225∼220 Ma.

Acknowledgements This study has been supported by funds from the Chinese Ministry of Science and Technology (G1999075503) and the Chinese Academy of Science (KXCZ2-107). Thanks are due to Dr. Bin Fu, Dr. Laili Jiang and Dr. Qingchen Wang for their assistance during the field trip, to Dr. Wen Chen and Dr. Yanbin Wang for their assistance with Ar–Ar and U–Pb dating. Comments by Prof. J.L.R. Touret, Dr. Yilin Xiao and a anonymous reviewer helped the improvement of the manuscript.

References

Ames L, Zhou G, Xiong B (1996) Geochronology and geochemistry of ultrahigh-pressure metamorphism with implications for collision of Sino-Korea Cratons, Central China. Tectonics 15:472–489

Atherton MP, Ghani AA (2002) Slab breakoff: a model for Caledonian, Late granite syn-collisional magmatism in the orthotectonic (metamorphic) zone of Scotland and Donegal, Ireland. Lithos 62:65–85

Austrheim H (1998) Influence of fluid and deformation on metamorphism of the deep crust and consequences for the geodynamics of collision zones. In: Hacker BR, Liou JG (eds) When continents collide: geodynamics and geochemistry of ultrahigh-pressure rocks. Kluwer, Dordrecht, pp 297–323

Ayers JC, Dunkle S, Gao S, Miller CF (2002) Constraints on timing of peak and retrograde metamorphism in Dabie Shan Ultrahigh-Pressure Metamorphic Belt, east central China, using U–Th–Pb dating of zircon and monazite. Chem Geol 186:315–331

Ballever M, Pitra P, Bohn M (2003) Lawsonite growth in the epidote blueschists from the Ile de Groix (Armorican Massif, France): a potential geobarometer. J Metamorph Geol 21:723–735

Barnicoat AC (1988) Zoned high-pressure assemblages in pillow lavas of the Zermatt-Saas ophiolite zone, Switzerland. Lithos 21:227–236

Barnicoat AC, Fry N (1986) High-pressure metamorphism in the Zermatt-Saas Fee ophiolite zone, Switzerland. J Geol Soc Lond 143:607–618

Caron J-M, Pequignot G (1986) The transition between blueschists and lawsonite-bearing eclogites base on observations from Corican metabasalts. Lithos 19:205–218

Carswell DA, O'Brien PJ, Wilson RN, Zhai M (1997) Thermobarometry of phengite-bearing eclogites in the Dabie Mountains of central China. J Metamorph Geol 15:239–252

Cartwright I, Buick IS (2000) Fluid generation, vein formation and the degree of fluid-rock interaction during decompression of high- pressure terranes: the Schistes Lustres, Alpine Corsica, France. J Metamorph Geol 18:607–624

Castelli D, Rolfo F, Compagnoni R, Xu ST (1998) Metamorphic veins with kyanite, zoisite and quartz in the Zhu-Jia-Chong eclogites, Dabie Shan, China. Island Arc 7:159–173

Chavagnac V, Jahn Bm (1996) Coesite-bearing eclogites from the Bixiling Complex, Dabie Mountains, China: Sm–Nd ages, geochemical characteristics and tectonic implications. Chem Geol 133:29–51

Chen W, Liu X-Y, Zhang S-H (2002) Continuous laser stepwise heating $^{40}Ar/^{39}Ar$ dating technique. Geol Rev 48(Suppl):127–134 (in Chinese with English abstract)

Chen J-F, Xie Z, Li H-M, Zhang X-D, Zhou T-X, Park Y-S, Ahn K-S, Chen D-G, Zhang X (2003) U–Pb zircon ages for a collision-related K-rich complex at Shidao in the Sulu ultrahigh pressure terrane, China. Geochem J 37:35–46

Clayton RN, Mayeda TK (1963) The use of bromine pentafluoride in the extraction of oxygen from oxides and silicates for oxygen isotope analysis. Geochim Cosmochim Acta 27:43–52

Compston W, Williams IS, Kirschvink JL, Zhang Z, Ma G (1992) Zircon U–Pb ages for the Early Cambrian time-scale. J Geol Soc London 149:171–184

Cong B-L (1996) Ultrahigh-Pressure Metamorphic Rocks in the Dabieshan-Sulu Region of China. Science Press, Beijing, p 224

Davies JH, von Blanckenburg F (1995) Slab breakoff: a model of lithosphere detachment and its test in the magmatism and deformation of collisional orogens. Earth Planet Sci Lett 129:85–102

DePaolo DJ (1988) Neodymium isotope geochemistry: an introduction. Springer, Berlin Heidelberg New York, p 181

Eiler JM, Farley KA, Valley JW, Stolper EM, Hauri E, Craig H (1995) Oxygen isotope evidence against bulk recycled sediment in the source of Pitcairn island lavas. Nature 377:138–141

Ernst WG (2001) Subduction, ultrahigh-pressure metamorphism, and regurgitation of buoyant crustal slices—implications for arcs and continental growth. Phys Earth Planet Inter 127:253–275

Forneris JF, Holloway JR (2003) Phase equilibria in subducted basaltic crust: implications for H_2O release from the slab. Earth Planet Sci Lett 214:187–201

Franz L, Romer RL, Klemd R, Schmid R, Oberhaensli R, Wagner T, Dong S (2001) Eclogite-facies quartz veins within metabasites of the Dabie Shan (eastern China): pressure-temperature-time-deformation path, composition of the fluid phase and fluid flow during exhumation of high-pressure rocks. Contrib Miner Petrol 141:322–346

Friedmann I (1953) Deuterium content of natural water and other substances. Geochim Cosmochim Acta 4:89–103

Fu B, Zheng Y-F, Wang Z-R, Xiao Y-L, Gong B, Li S-G (1999) Oxygen and hydrogen isotope geochemistry of gneisses associated with ultrahigh pressure eclogites at Shuanghe in the Dabie Mountains. Contrib Miner Petrol 134:52–66

Fu B, Touret JLR, Zheng Y-F (2001) Fluid inclusions in coesite-bearing eclogites and jadeite quartzite at Shuanghe, Dabie Shan (China). J Metamorph Geol 19:529–545

Fu B, Zheng Y-F, Touret JLR (2002) Petrological, isotopic and fluid inclusion studies of eclogites from Sujiahe, NW Dabie Shan (China). Chem Geol 187:107–128

Fu B, Touret JLR, Zheng Y-F, Jahn B-m (2003a) Fluid inclusions in granulites, granulitized eclogites, and garnet clinopyroxenites from the Dabie-Sulu terranes, eastern China. Lithos 70:293–319

Fu B, Touret JLR, Zheng Y-F (2003b) Remants of premetamorphic fluid and oxygen isotopic signatures in eclogites and garnet clinopyroxenite from the Dabie-Sulu terranes, eastern China. J Metamorph Geol 21:561–578

Graham CM (1981) Experimental hydrogen isotope studies III: diffusion of hydrogen in hydrous minerals, and stable isotope exchange in metamorphic rocks. Contrib Miner Petrol 76:216–228

Graham CM, Sheppard SMF, Heaton THE (1980) Experimental hydrogen isotope studies: I. Systematics of hydrogen isotope fractionation in the systems epidote-H_2O, zoisite-H_2O and AlO(OH)-H_2O. Geochim Cosmochim Acta 44:353–364

Graham CM, Harmon RS, Sheppard SMF (1984) Experimental hydrogen isotope studies: hydrogen isotope exchange between amphibole and water. Am Miner 69:128–138

Grevel K-D, Schoenitz M, Skrok V, Navrotsky A, Schreyer W (2001) Thermodynamic data of lawsonite and zoisite in the system $CaO–Al_2O_3–SiO_2–H_2O$ based on experimental phase equilibria and carorimetric work. Contrib Mineral Petrol 142:298–308

Hacker BR, Ratschbacher L, Webb LE, Ireland TR, Walker D, Dong S (1998) U/Pb zircon ages constrain the architecture of the ultrahigh-pressure Qinling-Dabie orogen, China. Earth Planet Sci Lett 161:215–230

van Haren JL, Ague JJ, Rye DM (1996) Oxygen isotope record of fluid infiltration and mass transfer during regional metamorphism of pelitic schist, Connecticut, USA. Geochim Cosmochim Acta 60:3487–3504

Hegner E, Walter HJ, Satir M (1995) Pb–Sr–Nd isotopic compositions and trace element geochemistry of megacrysts and melilities from the Tertiary Urach volcanic field: source composition of small volume melts under SW Germany. Contrib Miner Petrol 122:322–335

Henry C, Burkhard M, Goffe B (1996) Evolution of synmetamorphic veins and their wallrocks through a Western Alps transect: no evidence for large-scale fluid flow. Stable isotope, major and trace-element systematics. Chem Geol 127:81–109

Holland TJB (1980) The reaction albite = jadeite + quartz determined experimentally in the range 600–1200°C. Am Miner 65:129–134

Holland TJB, Powell R (1990) An enlarged and updated internally consistent thermodynamic data set with uncertainties and corrections: the system $K_2O–Na_2O–CaO–MgO–FeO–Fe_2O_3–Al_2O_3–TiO_2–SiO_2–C–H_2–O_2$. J Metamorph Geol 8:89–124

Holland TJB, Powell R (1991) A compensated-Redlich-Kwong (CORK) equation for volumes and fugacities of CO_2 and H_2O in the range 1 bar to 50 kbar and 100–1600°C. Contrib Miner Petrol 109:265–273

Holland TJB, Powell R (1998) An internally-consistent thermodynamic dataset for phases of petrological interest. J Metamorph Geol 16:309–343

Hoskin PWO (1998) Minor and trace element analysis of natural zircon ($ZrSiO_4$) by SIMS and laser ablation ICPMS: a consideration and comparison of two broadly comparative techniques. J Trace Microprobe Tech 16:301–326

Jahn B-M (1998) Geochemical and isotopic characteristics of UHP eclogites and ultramafic rocks of the Dabie orogen: implications for continental subduction and collisional tectonics. In: Hacker BR, Liou JG (eds) When continents collide: geodynamics and geochemistry of ultrahigh-pressure rocks. Kluwer, Dordrecht, pp 203–239

Katayama I, Nakashima S (2003) Hydroxyl in clinopyroxene from the deep subducted crust: evidence for H_2O transport into the mantle. Am Miner 88:229–234

Kretz R (1983) Symbols for rock-forming minerals. Am Miner 68:277–279

Lasaga AC (1983) Geospeedometry: an extension of geothermometry. In: Saxena SK (ed) Kinetics and equilibrium in mineral reactions. Advances in physical geochemistry, vol 3. Springer, Berlin Heidelberg New York, pp 81–114

Li S-G, Xiao YL, Liou DL, Chen YZ, Ge NJ, Zhang ZQ, Sun Ss, Cong BL, Zhang RY, Hart SR, Wang SS (1993) Collision of the North China and Yangtse Blocks and formation of coesite-bearing eclogites: timing and processes. Chem Geol 109:89–111

Li S-G, Wang SS, Chen YZ, Liu DL, Qiu J, Zhou XH, Zhang ZM (1994) Excess argon in phengite from eclogite: evidence from dating of eclogite minerals by Sm–Nd, Rb–Sr and $^{40}Ar/^{39}Ar$ methods. Chem Geol 112:343–350

Li S-G, Jagoutz E, Lo C-H, Chen YZ., Li Q-L, Xiao Y-L (1999) Sm/Nd, Rb/Sr, and $^{40}Ar/^{39}Ar$ isotopic systematics of the ultrahigh-pressure metamorphic rocks in the Dabie-Sulu belt, Central China: a retrospective view. Intern Geol Rev 41:1114–1124

Li S-G, Jagoutz E, Chen YZ, Li QL (2000) Sm–Nd and Rb–Sr isotopic chronology and cooling history of ultrahigh pressure metamorphic rocks and their country rocks at Shuanghe in the Dabie terrain, Central China. Geochim Cosmochim Acta 64:1077–1093

Li Y-L, Zheng Y-F, Fu B, Zhou J-B, Wei C-S (2001) Oxygen isotope composition of quartz-vein in ultrahigh-pressure eclogite from Dabieshan and implications for transport of high-pressure metamorphic fluid. Phys Chem Earth A 26:695–704

Liati A, Gebauer D (1999) Constraining the prograde and retrograde P-T-t path of Eocene HP rocks by SHRIMP dating of different zircon domains: inferred rates of heating, burial, cooling and exhumation for central Rhodope, northern Greece. Contrib Miner Petrol 135:340–354

Liou JG, Zhang RY, Eide EA, Wang XM, Ernst WG, Maruyama S (1996) Metamorphism and tectonics of high-pressure and ultra-high-pressure belts in the Dabie-Sulu region, China. In: Harrison MT, Yin A (eds) The tectonics of Asia. Cambridge University Press, London, pp 300–344

Liou JG, Zhang RY, Ernst WG, Rumble D, Maruyama S (1998) High-pressure minerals from deeply subducted metamorphic rocks. In: Mao HK, Hemley RJ (eds) Ultrahigh-pressure mineralogy. Rev Miner 37:33–96

Ludwig KR (2001) Users Manual for Isoplot/Ex (rev 2.49): a geochronological toolkit for microsoft excel. Berkeley Geochronology Center, Special Publication, vol 1a, p 55

Matthews A, Liati A, Mposkos E, Skarpelis N (1996) Oxygen isotope geochemistry of the Rhodope polymetamorphic terrain in northern Greece: evidence for preservation of pre-metamorphic isotopic composition. Eur J Miner 8:1139–1152

Nakamura D (2002) Kinetic of decompresional reactions in eclogitic rocks-formation of plagioclase coronas around kyanite. J Metamorph Geol 20:325–333

Okamoto K, Maruyama S (1999) The high-pressure synthesis of lawsonite in the MORB + H_2O system. Am Miner 84:362–373

Okay AI (1980) Minerals, petrology and phase relations of glaucophane-lawsonite zone blueschists from the Tavsanli Region, Northwest Turkey. Contrib Miner Petrol 72:243–255

Okay AI (1993) Petrology of a diamond-and coesite-bearing metamorphic terrain, Dabieshan, China. Eur J Miner 5:659–675

Okay AI, Sengor AMC, Satir M (1993) Tectonics of an ultra-high-pressure metamorphic terrane, the Dabie Shan/Tongbai Shan region, China. Tectonics 12:1320–1334

Pawley AR (1994) The pressure and temperature stability limits of lawsonite: Implications for H_2O recycling in subduction zones. Contrib Miner Petrol 118:99–108

Poli S, Schmidt MW (1997) The high-pressure stability of hydrous phases in orogenic belts: an experimental approach on eclogite-forming processes. Tectonophys 273:169–184

Powell R, Holland TJB (1988) An internally consistent thermodynamic dataset with uncertainties and correlations: 3. Applications to geobarometry, worked examples and a computer program. J Metamorph Geol 6:173–204

Roberts MP, Finger F (1998) Do U–Pb zircon ages from granulites reflect peak metamorphic conditions? Geology 25:319–322

Rowley DB, Xue F, Tucker RD, Peng Z, Baker J, Davis A (1997) Ages of ultrahigh pressure metamorphism and protolith orthogneisses from the eastern Dabie Shan: U/Pb zircon geochronology. Earth Planet Sci Lett 151:191–203

Rubatto D, Hermann J (2003) Zircon formation during fluid circulation in eclogites (Monviso, Western Alps): implications for Zr and Hf budget in subduction zones. Geochim Cosmochim Acta 67:2173–2187

Rubatto D, Gebauer D, Compagnoni R (1999) Dating of eclogite-facies zircons: the age of Alpine metamorphism in the Sesia-Lanzo Zone (Western Alps). Earth Planet Sci Lett 167:141–158

Rumble D, Yui T-F (1998) The Qinglongshan oxygen and hydrogen isotope anomaly near Donghai in Jiangsu Province, China. Geochim Cosmochim Acta 62:3307–3321

Rumble D, Giorgis D, Oreland T, Zhang Z-M, Xu H-F, Yui T-F, Yang J-S, Xu Z-Q, Liou JG (2002) Low $\delta^{18}O$ zircons, U–Pb dating, and the age of the Qinglongshan oxygen and hydrogen isotope anomaly near Donghai in Jiangsu province, China. Geochim Cosmochim Acta 66:2299–2306

Schmidt MW, Poli S (1998) Experimentally based water budgets for dehydrating slabs and consequences for arc magma generation. Earth Planet Sci Lett 163:361–379

Schulte B, Sindern S (2002) K-rich fluid metasomatism at high-pressure metamorphic conditions: lawsonite decomposition in rodingitized ultramafite of the Maksyutovo Complex, Southern Urals (Russia). J Metamorph Geol 20:529–541

Sharp ZD (1990) A laser-based microanalytical method for the in situ determination of oxygen isotope ratios of silicates and oxides. Geochim Cosmochim Acta 54:1353–1357

Sheng YM, Xia QK, Yang XZ (2004) Heterogeneity of water in UHP eclogites from Bixiling in Dabieshan: evidence from garnet. Chin Sci Bull 49:481–486

Spandler C, Hermann J, Arculus R, Mavrogenes J (2003) Redistribution of trace elements during prograde metamorphism from lawsonite blueschist to eclogite facies; implications for deep subduction-zone processes. Contrib Miner Petrol 146:205–222

Su W, Ji ZP, You ZD, Liu JB, Yu J, Cong BL (2004) Distribution of hydrous components in jadeite of the Dabie Mountains. Earth Planet Sci Lett 222:85–100

Sun WD, Li SG, Chen YD, Li YJ (2002) Timing of synorogenic granitoids in the south Qinling, central China: constraints on the evolution of the Qinling-Dabie orogenic belt. J Geol 110:457–468

Suzuoki T, Epstein S (1976) Hydrogen isotope fractionation between OH-bearing minerals and water. Geochim Cosmochim Acta 40:1229–1240

Terry MP, Robinson P, Krogh Ravna EJ (2000) Kyanite eclogite thermobarometry and evidence for thrusting of UHP over HP metamorphic rocks, Nordoyane, Western Gneiss Region, Norway. Am Miner 85:1637–1650

Valley JW, Kitchen N, Kohn MJ, Niendorf CR, Spicuzza MJ (1995) UWG-2, a garnet standard for oxygen isotope ratio: strategies for high precision and accuracy with laser heating. Geochim Cosmochim Acta 59:5223–5231

Vavra G, Schmid R, Gebauer D (1999) Internal morphology, habit and U-Th-Pb microanalysis of amphibolite-to-granulite facies zircons: geochronology of the Ivrea Zone (Southern Alps). Contrib Mineral Petrol 134:380–404

Wang XM, Liou JG, Maruyama S (1992) Coesite-bearing eclogites from the Dabie Mountains, Central China: petrology and P-T path. J Geol 100:231–250

Wang XM, Zhang RY, Liou JG (1995) UHPM terrane in east central China. In: Coleman R, Wang XM (eds) Ultrahigh Pressure Metamorphism. Cambridge University Press, London, pp 356–390

Webb LE, Hacker BR, Ratschbacher L, McWilliams MO, Dong S (1999) Thermo-chronological constraints on deformation and cooling history of high- and ultrahigh-pressure rocks in the Qinling-Dabie orogen, eastern China. Tectonics 18:621–638

Will T, Okrusch M, Schmaedicke E (1998) Phase relations in the greenschist-blueschist-amphibolite-eclogite facies in the system Na_2O–CaO–FeO–MgO–Al_2O_3–SiO_2–H_2O (NCFMASH), with application to metamorphic rocks from Samos, Greece. Contrib Mineral Petrol 132:85–102

Williams IS (1998) U–Th–Pb geochronology by ion microprobe. In: McKibben MA, Shanks III WC, Ridley WI (eds) Applications of microanalytical techniques to understanding mineralizing processes. Rev Econ Geol 7:1–35

Xiao Y-L, Hoefs J, van den Kerkhof AM, Fiebig J, Zheng Y-F (2000) Fluid history of UHP metamorphism in Dabie Shan, China: a fluid inclusion and oxygen isotope study on the coesite-bearing eclogite from Bixiling. Contrib Miner Petrol 139:1–16

Xiao Y-L, Hoefs J, van den Kerkhof AM, Simon K, Fiebig J, Zheng Y-F (2002) Fluid evolution during HP and UHP metamorphism in Dabie Shan, China: Constraints from mineral chemistry, fluid inclusions and stable isotopes. J Petrol 43:1505–1527

Yardley B, Gleeson S, Bruce S, Banks D (2000) Origin of retrograde fluids in metamorphic rocks. J Geochem Explor 69–70:281–285

Zhai M-G, Cong B-L, Zhao Z-Y (1995) Petrological-tectonic units in the coesite-bearing metamorphic terrain of the Dabie Mountains, central China and their geotectonic implications. J Southeast Asian Earth Sci 11:1–13

Zhang H-F, Zhong Z-Q, Gao S, Zhang B-R, Li HM (2001) U–Pb zircon age of the foliated garnet-bearing granites in western Dabie Mountains, central China. Chin Sci Bull 46:1657–1660

Zhang JF, Jin ZM, Green II HW, Jin SY (2001) Hydroxyl in continental deep subduction zone: evidence from UHP eclogites of the Dabie Mountains. Chin Sci Bull 46:592–595

Zhang JF, Green II HW, Bozhilov K, Jin ZM (2004) Faulting induced by precipitation of water at grain boundaries in hot subducting oceanic crust. Nature 428:633–636

Zheng Y-F (1991) Calculation of oxygen isotope fractionation in metal oxides. Geochim Cosmochim Acta 55:2299–2307

Zheng Y-F (1993a) Calculation of oxygen isotope fractionation in anhydrous silicate minerals. Geochim Cosmochim Acta 57:1079–1091

Zheng Y-F (1993b) Calculation of oxygen isotope fractionation in hydroxyl-bearing minerals. Earth Planet Sci Lett 120:247–263

Zheng Y-F, Fu B (1998) Estimation of oxygen diffusivity from anion porosity in minerals. Geochem J 32:71–89

Zheng Y-F, Fu B, Li Y-L, Xiao Y-L, Li S-G (1998) Oxygen and hydrogen isotope geochemistry of ultrahigh pressure eclogites from the Dabie Mountains and the Sulu terrane. Earth Planet Sci Lett 155:113–129

Zheng Y-F, Fu B, Xiao Y-L, Li Y-L, Gong B (1999) Hydrogen and oxygen isotope evidence for fluid-rock interactions in the stages of pre- and post-UHP metamorphism in the Dabie Mountains. Lithos 46:677–693

Zheng Y-F, Wang Z-R, Li S-G, Zhao Z-F (2002) Oxygen isotope equilibrium between eclogite minerals and its constraints on mineral Sm–Nd chronometer. Geochim Cosmochim Acta 66:625–634

Zheng Y-F, Fu B, Gong B, Li L (2003a) Stable isotope geochemistry of ultrahigh pressure metamorphic rocks from the Dabie-Sulu orogen in China: Implications for geodynamics and fluid regime. Earth Sci Rev 62:105–161

Zheng Y-F, Gong B, Zhao Z-F, Fu B, Li Y-L (2003b) Two types of gneisses associated with eclogite at Shuanghe in the Dabie terrane: carbon isotope, zircon U–Pb dating and oxygen isotope. Lithos 70:321–343

Zheng Y-F, Zhao Z-F, Li S-G, Gong B (2003c) Oxygen isotope equilibrium ultrahigh-pressure metamorphic minerals and its constraints on Sm–Nd and Rb–Sr chronometers. In: Vance D, Muller W, Villa I (eds) Geochronology: linking the isotope record with petrology and textures. Geol Soc Spec Publ 220:93–117

Zheng Y-F, Yang J-J, Gong B, Jahn B-m (2003d) Partial equilibrium of radiogenic and stable isotope systems in garnet peridotite during UHP metamorphism. Am Miner 88:1633–1643

Zheng Y-F, Wu Y-B, Chen FK, Gong B, Li L, Zhao Z-F (2004) Zircon U–Pb and oxygen isotope evidence for a large-scale ^{18}O depletion event in igneous rocks during the Neoproterozoic. Geochim Cosmochim Acta 68:4159–4179